
This is an electronic reprint of the original article.
This reprint may differ from the original in pagination and typographic detail.

Abed, Ayman; Sołowski, Wojciech Tomasz

Estimation of water retention behaviour of bentonite based on mineralogy and mercury intrusion porosimetry tests

Published in:
Géotechnique

DOI:
[10.1680/jgeot.18.P.220](https://doi.org/10.1680/jgeot.18.P.220)

Published: 01/06/2021

Document Version
Peer-reviewed accepted author manuscript, also known as Final accepted manuscript or Post-print

Please cite the original version:
Abed, A., & Sołowski, W. T. (2021). Estimation of water retention behaviour of bentonite based on mineralogy and mercury intrusion porosimetry tests. *Géotechnique*, 71(6), 494-508. Article 220.
<https://doi.org/10.1680/jgeot.18.P.220>

This material is protected by copyright and other intellectual property rights, and duplication or sale of all or part of any of the repository collections is not permitted, except that material may be duplicated by you for your research use or educational purposes in electronic or print form. You must obtain permission for any other use. Electronic or print copies may not be offered, whether for sale or otherwise to anyone who is not an authorised user.

Accepted manuscript doi: 10.1680/jgeot.18.P.220

Accepted manuscript

As a service to our authors and readers, we are putting peer-reviewed accepted manuscripts (AM) online, in the Ahead of Print section of each journal web page, shortly after acceptance.

Disclaimer

The AM is yet to be copyedited and formatted in journal house style but can still be read and referenced by quoting its unique reference number, the digital object identifier (DOI). Once the AM has been typeset, an 'uncorrected proof' PDF will replace the 'accepted manuscript' PDF. These formatted articles may still be corrected by the authors. During the Production process, errors may be discovered which could affect the content, and all legal disclaimers that apply to the journal relate to these versions also.

Version of record

The final edited article will be published in PDF and HTML and will contain all author corrections and is considered the version of record. Authors wishing to reference an article published Ahead of Print should quote its DOI. When an issue becomes available, queuing Ahead of Print articles will move to that issue's Table of Contents. When the article is published in a journal issue, the full reference should be cited in addition to the DOI.

Accepted manuscript doi: 10.1680/jgeot.18.P.220

Submitted: 07 September 2018

Published online in 'accepted manuscript' format: 10 March 2020

Manuscript title: Estimation of water retention behaviour of bentonite based on mineralogy and mercury intrusion porosimetry tests

Authors: Ayman A. Abed* and Wojciech T. Sołowski*

Affiliation: *Department of Civil Engineering, Aalto University, Espoo, Finland

Corresponding author: Ayman A. Abed, Department of Civil Engineering, Aalto University, P.O. Box 12100, FI-00076 Aalto, Finland. Tel.: +358 50 4088908.

E-mail: ayman.abed@aalto.fi

Abstract

This paper develops a water retention model based on the soil mineralogy and microscopic features of the material behaviour. The model estimates the water content at a given total suction as the sum of the bentonite minerals interlayer water and the water in the interparticle pores. The paper proposes simple formulae to estimate the interlayer water content and interlayer void ratio based on mineralogical properties. Additionally, the model uses the mercury intrusion porosimetry measurements to approximate the water content in the larger pores. The validation of the proposed procedure relies on published data for MX-80 and GMZ bentonites and yields promising results. Even though the discussion and the validation are restricted to bentonite here, the procedure is generic in nature and can be modified easily for other geomaterials. The paper also offers insights into the links between soil microstructure and its macroscopic behaviour. The contribution provides a new tool for quick indirect estimation of the water retention behaviour of porous materials with known mineral composition and available microstructural data, e.g. based on the mercury intrusion porosimetry tests. Such tool is of high practical interest in design e.g. nuclear waste repositories where large material pool may be initially considered.

INTRODUCTION

The soil water retention curve characterises the ability of a particular porous material to hold water at a given suction value (s). Usually it is defined as a continuous relationship between suction and water content (w), or between suction and degree of saturation (S^l) (Fredlund & Rahardjo, 1993). This relationship, being also known as soil water characteristic curve (SWCC), is a fundamental constitutive equation which plays a central role in the Thermo-Hydro-Mechanical-Chemical (THMC) coupled behaviour of unsaturated porous material (Abed & Sołowski, 2017). The correct estimation of the water retention curve is especially important for clay-rich materials such as bentonite, due to high water retaining ability under high suction resulting in a very low hydraulic conductivity. Low conductivity, self-sealing ability due to swelling, together with durability typical to natural mineral materials, lead to bentonite being the material to be used for the sealing of high-level nuclear waste (Bucher *et al.*, 1989; Sellin & Leupin, 2013; Pusch, 2015). Due to the complex surrounding environmental conditions, as well as the time scale, the design of such repository requires accurate prediction of the material behaviour and thus the solution of Thermo-Hydro-Mechanical-Chemical coupled balance equations with advanced numerical methods (Olivella *et al.*, 1996; Thomas & He, 1997; Collin *et al.*, 2002; Wu *et al.*, 2004; Abed & Sołowski, 2017). This paper presents a new water-retention model that links the water retention behaviour of the soil to the minerals present in the material, as well as to the pore size distribution. The inclusion of microstructure leads to a more accurate understanding of the material evolution caused by wetting and drying or by other factors that influence the water retention curve. It also opens up the constitutive modelling of clay to the wealth of information about the material microstructure coming from the experiments as well as numerical methods such as molecular dynamics. Inclusion of the microstructure related

knowledge from physics and chemistry would give the THMC framework an additional physical basis and an extra link (and associated limits related to material behaviour) between material macroscopic behaviour and its microstructure and mineralogy. For example, pore structure may be linked with transport properties and material parameters, leading to an increase of the reliability of the long-term predictions, as one would have physical link instead of uncertain parameter values.

There are several methods to obtain the water retention curve (Zielinski *et al.*, 2010), though the related tests are usually time consuming and relatively expensive. In general, the water retention curve shows irreversible hysteric behaviour during drying and wetting. The hysteresis is attributed to several reasons including the non-uniformity of the pores leading to the inkbottle effect, the difference in contact angle in wetting and drying phases and the entrapped air within the pores during drying process (Haines, 1930). The accumulated research data also reveal other factors that influence the water retention curve including, but not restricted to: i) initial dry density (void ratio), ii) temperature, iii) chemical and salt concentration (Jacinto *et al.*, 2009; Kuusela-Lahtinen *et al.*, 2016). Ideally, all the aforementioned factors should be addressed during modelling.

As the laboratory tests measure a limited number of points of the water retention curve, to get a continuous curve suitable for numerical implementation in a THMC code, one fits the experimental data with a mathematical function. Leong & Rahardjo (1997) provide a detailed review of the classical formulae for the soil water characteristic curves. Initially, the aim of the majority of these expressions was to fit data for common agricultural and geotechnical practical applications, hence they assume the water retention curve to be constant throughout the analysis (Fredlund & Rahardjo, 1993). However, in special engineering applications,

where there is a need to consider the complex coupling between the mechanical, hydraulic, thermal and chemical effects on the material, classical models limitations emerge.

It now seems that to capture the THMC effects accurately, one has to account for the microstructural influence on the overall material behaviour (Gens & Alonso, 1992; Delage *et al.*, 2006; Tarantino, 2009; Romero *et al.*, 2011; Musso *et al.*, 2013; Seiphoori *et al.*, 2014; Della Vecchia *et al.*, 2015), which is a significant challenge.

Fig. 1 illustrates a schematic representation of the pore structure in a clay-rich soil. Taking the pore-diameter D as the classification criterion, three structural levels may be distinguished (Romero, 1999; Delage *et al.*, 2006; Monroy *et al.*, 2010; Seiphoori *et al.*, 2014):

- (a) Macro-level (inter-aggregate pores): includes all the pores with diameter larger than approximately 200nm (0.2 μ m).
- (b) Micro-level (intra-aggregate pores): typically gathers all the pores with diameter in the range [1.2nm (12Å)-200nm].
- (c) Intra-particle level: includes the interlayer spaces, which vary depending on the degree of saturation. At full saturation, it contains all the spaces with interlayer distance less than 1.2nm (12Å).

It is worthwhile to mention that the provided limits to distinguish these structural levels are approximate and generally depend on the tested material. They are given here mainly to give an example of the typical pore size ranges.

The mercury intrusion porosimetry (MIP) test results give information on the microstructure of the porous material. Depending on the used apparatus, MIP allows to investigate pore diameters in the range 4nm ~ 400 μ m which covers the structural levels *a* and *b*.

As discussed later in the paper, MIP can help in estimation of the drying branch of soil water retention curve (Romero *et al.*, 1999; Simms & Yanful, 2002; Nowamooz & Masrouri, 2010; Della Vecchia *et al.*, 2015). The existing water retention models (Romero *et al.*, 1999; Simms & Yanful, 2002; Nowamooz & Masrouri, 2010) which use MIP data, rely on the porosimetry measurements only, without any in-depth consideration of the mineralogy effect on the interlayer water (structural level c that is not detected by MIP) or discussion of the effect of freeze-drying on the fabric structure before any mercury intrusion takes place. For instance, Romero *et al.* (1999) proposed an expression, that has been later adopted by Nowamooz & Masrouri (2010), to estimate the water retention curve based on MIP data. The expression contains a term that accounts for the residual water content that resides in the structural level c . However, that term has no derivation shown and is treated just as a fitting parameter. The mentioned existing models, which rely on porosimetry, can be quite accurate when the amount of this residual water content is negligible, that is in relatively coarse materials with low specific surface. However, for the materials that have large specific surface (such as bentonite), with the majority of water stored in the interlayers, the mercury intrusion porosimetry test alone is insufficient to reproduce the water retention properties. That is due to both the sample preparation procedures, and the test itself, as MIP does not allow for an accurate assessment of the sizes of interlayer pores.

Saiyouri *et al.* (2000), Likos & Wayllace (2010), Villar *et al.* (2012) and Bestel *et al.* (2014) provided data about the evolution of interlayer water content in bentonite. However, these data, so far, have not been used to improve the existing soil water characteristic curve models. Therefore, this paper employs these data to introduce a novel procedure for estimating the water retention curve. Additionally, the proposed model accounts for the mineralogical properties of the material, such as its specific surface, as well as the

information related to the pore structure, obtained e.g. from the mercury intrusion porosimetry tests.

This study divides the total water content into the interlayer water content, consisting of water in between elementary clay layers and the interparticle water content, entailing water outside the particles. The model estimates the interlayer water content based on the basal distance between the clay particles and the specific surface of the bentonite, whereas the interparticle water content is estimated based on the MIP results. The paper proposes new formulae, e.g. to determine the interlayer water content, and computes the total water content as the total of the interlayer water content and the scaled interparticle water content obtained from MIP. The introduction of the scaling is justified by the need to compensate for the shrinkage happening at the clay particle level during the freeze-drying of the sample.

The proposed framework is validated against experimental data and gives very promising results. In principle, the approach is generic and can be used for any clay geomaterial, which has significant amount of water captured in the clay interlayer. The authors stress, however, that this method is not proposed, by any means, to replace the direct measurements of the SWCC but rather as a supporting tool for indirect estimation of the retention properties, especially useful in cases when the direct measurements of water retention behaviour are not available, or not feasible due to time constraints and costs (e.g. in preliminary estimation of properties during initial material pre-selection for large engineering projects).

WATER IN GRANULAR MATERIALS

When a conventional dry granular material is wetted, the water fills the smallest pores first followed by the larger ones until reaching full saturation. However, the water in the interlayer pores is chemically bound to the bentonite. The amount of this chemically bound water particles is in equilibrium with the water in the other pores and thus is linked to the total

suction value, but is not directly related to the pore size. Therefore, the interlayer pores may still not be filled with the maximum number of water particles before some of the other pores are filled with water.

This paper in particular is focused on bentonite applied to the sealing of nuclear waste storages, which tends to be saturated at almost constant volume. Such bentonite does not follow the classical wetting curve. Similarly, in these applications, the cycles of wetting and drying are not expected; hence, the hysteric behaviour is neglected at this stage of the study. These assumptions are supported by several experimental findings on the slight observed hysteresis in the SWCC of illite and montmorillonite-rich materials (Branson & Newman, 1983; Kraehenbuehl *et al.*, 1987; Delage *et al.*, 1998; Gens & Alonso, 1992).

It is also assumed that the water resides only in two main domains: i) the interlayer spaces (structural level *c*), where it is named as *interlayer water* (w_{int}) and ii) in the pores outside the interlayer spaces (structural levels *a* and *b*), consisting of intra- and inter-aggregate pores, where it is referred to as *interparticle water*. A fundamental assumption here is that the water in these two spaces are considered to be in hydraulic and chemical equilibrium so that they have the same total suction value at any point in time. Consequently, the total degree of saturation S^l is expressed as:

$$S^l = S_{int} + S_{out} \quad (1)$$

where S_{int} and S_{out} represent the contribution of the interlayer water and the interparticle water to the total degree of saturation, respectively. The interlayer water content contribution is defined as:

$$S_{int} = \frac{w_{int}}{w_{sat}} \quad (2)$$

where w_{sat} is the saturated water content of the geomaterial. The interparticle water contribution S_{out} is derived based on MIP data.

This paper aims to give a method to quantify these two components of water content, as well as to show how those can help in estimation of the soil water retention curve. The following section explains a simplified yet efficient method to estimate the *interlayer water contribution* based on mineralogy. Other, though comparable, derivation of this quantity is given in Tournassat & Appelo (2011). A later section shows how to estimate the *interparticle water contribution* based on mercury intrusion porosimetry measurements.

SIMPLIFIED METHOD TO ESTIMATE INTERLAYER WATER CONTENT AND POROSITY

The total specific surface S_s is the ratio of the surface area of a material to its mass. For a soil sample, it can be estimated based on the direct experimental measurements. Theoretically, with reference to Fig. 2, a clay sample composed from a single mineral has the total specific surface

$$S_s = NA \times L \times A_l \quad (3)$$

where NA is the total number of clay particles per unit mass of the material, L is the total number of layers per one clay particle and A_l is the surface area of one clay layer. Fig. 2 provides an additional explanation of the symbols.

Consequently, assuming that the available interlayer spaces is fully saturated at any total suction value, the water content in the interlayer w_{int} is:

$$w_{int} = \underbrace{0.5 \times NA \times A_l \times [2n + (L - 1)m]}_{\text{interlayer volume occupied by water per unit mass}} \times \rho_w^{int} \quad (4)$$

where n and m are the number of water layers on the external and internal surface of a single clay particle, respectively (see Fig. 2 for more clarification). The symbols δ_w and ρ_w^{int} denote the thickness of one water layer and the interlayer water density, respectively.

Taking into account the expression for the specific surface in Equation (3) one finds:

$$w_{int} = 0.5 \times \frac{S_s}{L} \times [2n + (L - 1)m] \times \delta_w \times \rho_w^{int} \quad (5)$$

For the clay particles $L \gg n$ and $L \gg 1$ (Saiyouri *et al.*, 2000), which allows for a simplification $\frac{2n}{L} \approx 0$ and $\frac{L-1}{L} \approx 1$, leading to:

$$w_{int} = 0.5 \times S_s \times \delta_{int} \times \rho_w^{int} \quad (6)$$

The symbol $\delta_{int} = m \times \delta_w$ represents the interlayer distance which is mineral and saturation dependent (Saiyouri *et al.*, 2000; Likos & Wayllace, 2010; Villar *et al.*, 2012; Bestel *et al.*, 2014).

For a soil that consists of more than a single mineral (let J be the total number of composing minerals), Equation (6) becomes:

$$w_{int} = \sum_{i=1}^J w_{int,i} \times R_i \quad (7)$$

where R_i is the percentage of the i^{th} composing mineral by weight of total solids and $w_{int,i}$ is the interlayer water content of the i^{th} composing mineral calculated according to Equation (6).

Equation (7) demonstrates that the total water content in the interlayer w_{int} is the sum of the contribution of the interlayer water content for all the composing minerals ($i = 1 \dots J$). In this case, S_s and δ_{int} are mineral dependent and should be correctly considered during $w_{int,i}$ calculation.

In what follows the interlayer water density is assumed to be constant $\rho_w^{int} = 1.0\text{Mg/m}^3$ which is a first order approximation (Jacinto *et al.*, 2012; Marcial, 2011).

Fig. 3 compiles the measured interlayer distance δ_{int} versus suction in case of MX-80 bentonite conditions (Bestel *et al.*, 2014; Saiyouri *et al.*, 2000), similar data can also be found in Villar *et al.* (2012) and Chipera *et al.* (1998). It is worth mentioning that molecular dynamics simulations produce comparable data (Hsiao & Hedström, 2017) which provide a promising tool that might be utilized to generalize the method in the future. The measured data points were fitted by employing the least squares method, assuming an exponential fitting function of the form:

$$\delta_{int} = A e^{B s}, \quad (8)$$

where the total suction s is estimated in kPa. The analysis led to the values of fitting parameters $A = 9.237$ [Å] and $B = -1 \times 10^{-5}$ [1/kPa].

Combining the data depicted in Fig. 3 with Equation (7) for MX-80 bentonite with $R = 82\%$ montmorillonite and specific surface of $S_s = 522\text{m}^2/\text{g}$ (Delage *et al.*, 2006) gives the interlayer water content as shown in Fig. 4 with respect to suction. The suction appears here through the dependency of δ_{int} on suction in Equation (8). It is assumed that other composing minerals of bentonite have marginal effect on the interlayer water content and as such, they were neglected with $J = 1$ in this case. Obviously, the curve linking suction and interlayer water content is material dependent. For materials with a low specific surface, the interlayer water content will be low as well and the interlayer spacing will be smaller. For example, if the specific surface of MX-80 bentonite would be much lower, e.g. $40\text{m}^2/\text{g}$ (typical value for kaolinite), its interlayer water content would be much lower (see Fig. 4).

The interlayer water in Equation (7) shows significant dependency on the specific surface of the material. This is in line with the experimental findings provided by other researchers (e.g. Marinho, 2005) who found that the clay ability to hold water at high suction values is commensurate with the liquid limit w_L and consequently the specific surface. Unfortunately, the data provided by Marinho (2005) is for common clays with maximum $w_L < 120\%$. Bentonite has $w_L > 300\%$ and therefore no meaningful comparison is possible at this stage. Once the proposed method in this paper is generalised, such statistical method would be of significance for validation purposes.

Based on the fundamental relationships between the soil physical properties (Holtz & Kovacs, 1981), the interlayer water content w_{int} relates to the interlayer void ratio e_{int} and the interlayer porosity n_{int} as follows:

$$e_{int} = \frac{\rho_s}{\rho_w} w_{int}; \quad n_{int} = \frac{e_{int}}{1 + e_o}; \quad \rho_s = (1 + e_o)\rho_d \quad (9)$$

where ρ_s , ρ_d and e_o are the solid particles density, dry density and total void ratio, respectively.

Substituting Equation (7) into Equation (9) yields the following formula for the interlayer porosity:

$$n_{int} = \frac{\rho_d}{\rho_w} \sum_{i=1}^J w_{int,i} \times R_i \quad (10)$$

Equation (10) predicts the evolution of the interlayer porosity with the interlayer water content that leads implicitly to a relationship with suction. In case of compacted MX-80 bentonite, with $\rho_d = 1.6\text{Mg/m}^3$, the estimated interlayer porosity is depicted in Fig. 4. For a natural wet soil sample, at any given suction value, the interlayer porosity is fully occupied by chemically bound water. The interlayer pores are also very small, both of which

would mean that mercury might not be able to intrude these pores. Consequently, the non-intruded porosity during the porosimetry test should be always bigger or equal to that in Equation (10) and the measured soil water characteristic curve for the material should never fall below the limiting curve represented by S_{int} . However, the mercury intrusion tests a (freeze) dried material, meaning that there should be almost no water in the interlayer pores. In such case, the distance between clay platelets will be reduced, leading to a redistribution of the interlayer porosity into the larger pores.

ESTIMATION OF THE INTERPARTICLE WATER CONTENT FROM THE MERCURY INTRUSION POROSIMETRY RESULTS

The mercury intrusion porosimetry (MIP) investigates the distribution of pores in a porous material (Romero & Simms, 2008). The experiment is standardized (ASTM 4404-84, 1998), routinely used in practice and allows for the detection for pores as small as 4.0nm in diameter. However, no information about the smaller pores can be extracted from MIP data. The main idea behind MIP is to inject mercury (non-wetting fluid) gradually into a completely dried soil sample under increasing external pressure. The measured volume of the injected mercury and the corresponding applied pressure correlate to the pore volume and pore diameter, respectively (Prapaharan *et al.*, 1985). That eventually gives information about soil fabric and grain size distribution. Mercury intrusion into a completely dry sample resembles the intrusion of air into a fully saturated soil on drying path. Therefore, in principle, the derived retention properties based solely on MIP results correspond to the desorption curve. In addition, the mercury intrusion porosimetry theory assumes that all the pores in the tested material can be characterized as cylindrical with the diameter D . Usually in geotechnical applications, the MIP measurements are given as the mercury intruded void ratio e_{in} versus pore diameter. This value relates to the degree of saturation as follows:

$$e_{in} = \frac{V_{in}}{V_s} = \frac{V_v V_{in}}{V_v V_s} = \frac{V_v V_{in}}{V_s V_v} = e_o S_{in} = e_o(1 - S_{MIP}) \quad (11)$$

and consequently:

$$S_{MIP} = 1 - \frac{e_{in}}{e_o} \quad (12)$$

where V_{in} , V_v , V_s , e_o are the intruded void volume, the total void volume, the total solid particles volume and the total initial void ratio, respectively. The symbols S_{in} and S_{MIP} denote the mercury degree of saturation and the corresponding water degree of saturation as predicted by MIP, respectively.

The equivalent pore diameter D is linked to the corresponding suction s through the Washburn's equation (Washburn, 1921):

$$s = \frac{C}{D}; \quad (13)$$

where $C = 4 \sigma_t \cos(\alpha_c)$ is a constant for a given liquid. The symbol σ_t represents the surface tension of the pore fluid (for water, $\sigma_t = 0.07275\text{N/m}$) and α_c is the contact angle between the fluid and the soil particle. Typically for water-soil contact, α_c is taken as 0.0° which is a widely accepted assumption. There is still some discussion about the correct value of the contact angle to be adopted (Lourenço *et al.*, 2012). For example Zheng & Zaoui (2017) reported an angle as high as 25° in case of water-montmorillonite contact. However, in the investigated case of bentonite, most of water is residing in the interlayer spaces and the value of the adopted contact angle has only minor effect on the estimated water retention curve. Nonetheless, in case of coarser geomaterials where the role of capillary forces is dominant, the correct choice of contact angle would affect the predictions significantly.

Given the MIP measurements, the degree of saturation S_{MIP} at any D or s can be estimated with Equations (12) and (13). This value is later employed to estimate the interparticle water contribution S_{out} to the total degree of saturation S^l .

Arguing on the technical details of the mercury intrusion porosimetry test is out of the scope of this study and can be found elsewhere, e.g. in Ritter & Erich (1948), ASTM 4404 (1998) and Romero & Simms (2008). However, it is important to note that before the mercury intrusion starts, the sample has to be moisture free. That is achieved, in case of tests on bentonite, with a freeze-drying technique, in which the water is removed from the sample via sublimation. The technique seems to be able to remove all the water that is both the interparticle and the interlayer water from the sample. The effects of such sample preparation on the MIP test results are rarely discussed in the geotechnical field. Considering the interlayer pore spaces, the removal of water molecules would most likely result in altering the sample condition, as the interlayer space should close. That also alters the interlayer porosity (Murray & Quirk, 1980; Gallé, 2001; Saranya & Arnepalli, 2018) and eventually by the end of freeze-drying, the interlayer spaces will be smaller than in the initial sample. Here, we assume that they will be approximately 0.4\AA , which is the width of the interlayer space in a fully dry montmorillonite. There is a general agreement within the field that the freeze-drying followed by MIP intrusion would not affect the original clay pore structure (Sills *et al.*, 1973; Lawrence, 1978; Delage & Lefebvre, 1984), that is the pores which are above 4.0nm . However, it should be noted that these studies concentrated on the effect of mercury intrusion phase on the pore structure and not on the freeze-drying effect. Therefore, their findings are applicable to the sample after the freeze-drying procedure, during which the change of the interlayer spaces has already occurred. Furthermore, several experimental observations by Tovey (1971), Greene-Kelly (1973), Lawrence *et al.* (1979) and Wierzchoś *et al.* (1992)

support the hypothesis that it may be that the closure of interlayer spaces would eventually be reflected globally altering the whole pore structure of the material, especially where interlayer role is dominant (bentonite-like materials with large specific surface). Heller-Kallai in Bergaya and Lagaly (2013) states, as an undisputed fact, that freeze-drying stimulates edge-to-face association which alters the texture of the clay minerals creating a range of larger pores. Finally, Deirieh *et al.* (2018) provided excellent experimental data, which clearly showed that the freeze-drying affects the pore size distribution of clay. Further research quantifying the interlayer shrinkage effect on the interparticle level would be needed to shed more light on the issue.

As discussed in the introduction, it seems that the MIP results can be interpreted directly to predict the SWCC in case of coarse grain materials with relatively low specific surface. This has been indicated in Prapaharan *et al.* (1985), Romero *et al.* (1999) and Nowamooz & Masrouri (2010), where the ad-hoc values are assumed to calculate the residual water content which represents the interlayer water content. The materials with low specific surface are dominated by the capillary mechanism of water retention, which correlates to MIP data in a more physically sound way than in the case of materials with large specific surface that promotes the hydro-chemical activity (dominated by adsorption mechanism for retaining water). Perhaps, mercury intrusion porosimetry should be considered only as a supporting test in the case of bentonite-like materials, as it is not sufficient to give the complete picture of material porosity and hence water retention behaviour.

Despite this uncertainty, the accumulated MIP studies revealed, qualitatively, many interesting features of clay response under different hydro-mechanical paths (Delage *et al.*, 2006; Romero *et al.*, 2011; Della Vecchia *et al.*, 2015). The most relevant to the content of this paper are:

- a- Compacted clays are usually characterised by bimodal pore size distribution reflecting the concentration of pore diameters around two sizes. One representing the macro pores and the other the micro pores.
- b- External mechanical loading only affects the macro pores with marginal effect on the micro level pores. That explains the dependency of air entry value on the dry density of the soil.
- c- Drying path decreases both macro and micro pores volume and shift them towards smaller sizes.
- d- Under constant void ratio, saturation causes increase in micro pores volume and reduction in macro pores volume.
- e- At full saturation the pores tend to concentrate at a unified median pore range and the pore size distribution becomes single pore mode.
- f- Drying the sample again after full saturation will recover the bimodal distribution.

These observations have significant consequences on understanding and modelling the coupled hydro-mechanical behaviour of unsaturated soils. Most important for this paper, they show that the pore size distribution is not constant and consequently a single MIP measurement only represents one hydro-mechanical state, therefore, it is not enough to derive the full SWCC.

It is important to note that neither MIP measurements (due to insufficient intrusion pressure) nor the interlayer water content formula (7) gives data related to the water content in the range $12\text{\AA} - 40\text{\AA}$. Therefore, in this paper the amount of those pores will be extrapolated based on MIP results.

PREDICTION OF THE SOIL WATER CHARACTERISTIC CURVE

The problem associated with the derivation of the interparticle water contribution based on MIP results is that MIP is performed on a water-free sample and consequently its results employ the initial void ratio e_o as a reference value to estimate pore size distribution.

However, with reference to Fig. 5, in a hypothetical wet sample, which has not been treated with the freeze-drying technique, the void available for intrusion is considerably different due to the interlayer water. The amount of interlayer water, in a wet sample, increases nonlinearly with saturation (see Fig. 6 and Equation (7)) and simultaneously occupies increasing volume. Therefore, with the interlayer void ratio e_{int} in a hypothetical wet sample, estimated based on the simplified model introduced earlier, the void ratio available for MIP (intrusion) under constant volume is $e_{out} = e_o - e_{int}$. To consider this effect, the degree of saturation S_{MIP} derived based on MIP and e_o is scaled down by a factor α giving the contribution of the interparticle water $S_{out} = \alpha S_{MIP}$ to the total degree of saturation. The factor α is a variable controlled by the interlayer void ratio:

$$\alpha = \frac{e_o - e_{int}}{e_o} \quad (14)$$

This factor plays a role similar to an interaction function between micro and macro levels, a concept that is already used in several well-established modelling frameworks of unsaturated swelling clays (Gens & Alonso, 1992; Monroy *et al.*, 2010; Romero *et al.*, 2011; Della Vecchia *et al.*, 2015).

The total degree of saturation S^l at any suction is the sum of interlayer contribution S_{int} and the interparticle contribution S_{out} , see Fig. 6:

$$S^l = S_{int} + S_{out} = S_{int} + \alpha S_{MIP} \quad (15)$$

The effect of scaling gets smaller with the increasing coarseness of the material (decreasing specific surface). The assumed scaling is a simplification that may be improved in the future research; however, it seems to be sufficient for materials with high clay content.

Fig. 7 illustrates the evolution of α with suction for the MIP data obtained from MX-80 bentonite sample tested at initial degree of saturation of $S_o^l = 0.59$ (Delage *et al.*, 2006). The figure also gives S_{MIP} , the degree of saturation derived based on MIP and S_{out} , the corresponding scaled value. The authors emphasize that the data in Fig. 7 are only valid for $S^l = 0.59$. At other degrees of saturation, the MIP results differ and the resulted S_{out} differs. Each MIP test provides data to locate a single point on the SWCC. Table 1 lists the required steps to estimate that point at a given total degree of saturation.

One repeats the Steps 1 to 4 for other available MIP data at other initial total degrees of saturation to estimate other points on the SWCC. As a final simple step, these points can be used to fit a water retention curve with any suitable model (Leong & Rahardjo, 1997).

The ability of the framework to predict the soil water characteristic curve is assessed based on three different MIP data sets on MX-80 and GMZ bentonites provided by Delage *et al.* (2006), Ye *et al.* (2009), Seiphoori *et al.* (2014) and Lui (2016). These sets of data include measurements for the water retention curve, which are used for the validation purposes.

VALIDATION BASED ON DATA FROM Delage *et al.* (2006)

Within a comprehensive microstructural study on the effect of aging on the structure of compacted MX-80 Wyoming bentonite, Delage *et al.* (2006) provided MIP measurements performed on samples with dry density $\rho_d = 1.61 \text{Mg/m}^3$ at different initial (i.e. before freeze-drying) degrees of saturation. The maximum applied mercury intrusion pressure corresponded to the minimum detected pore diameter of $D = 6.8 \text{nm}$. Relevant physical properties of the investigated bentonite are as listed in Table 2.

Delage *et al.* (2006) also provided measured wetting branch of the SWCC under constant volume using vapour equilibrium method for a sample with $\rho_d = 1.7\text{Mg/m}^3$. Unfortunately, this dry density differs from the dry density used in the MIP, which makes the comparison difficult. To overcome that, additional data from Villar *et al.* (2005) also under constant volume but with $\rho_d = 1.6\text{Mg/m}^3$ and 1.7Mg/m^3 are considered in this example.

There is also an additional inconsistency in the SWCC data in Delage *et al.* (2006) where the curve is provided as water content w - suction s relationship. Here, the curve is converted to its degree of saturation S^l - suction s counterpart. However, for $\rho_s = 2.65\text{Mg/m}^3$ and $\rho_d = 1.7\text{Mg/m}^3$ the corresponding void ratio is $e = \rho_s/\rho_d - 1.0 = 2.65/1.7 - 1.0 = 0.559$. That yields a saturated water content of $w_{sat} = S^l e/G_s = 1.0 \times 0.559/2.65 = 0.21$ which is remarkably less than 0.25 the value provided by Delage *et al.* (2006). The difference might be attributed to the variation of water density ρ_w with saturation as has been discussed in Marcial (2011) and Jacinto *et al.* (2012) or some mistake. However, if the dry density of the bentonite was rather closer to 1.6 instead of 1.7, it would lead to almost perfect match with the saturated water content of 0.25, as well as lead to a match with the water retention curve of Villar *et al.* (2005) for the dry density of 1.6Mg/m^3 . This study assumes that $w_{sat} = 0.25$ which is used to convert the water content values as reported by Delage *et al.* (2006) to the corresponding degree of saturation.

The results of MIP tests for the samples with $\rho_d = 1.61\text{Mg/m}^3$ are given in the original contribution in terms of accumulated intruded void ratio for a sample with initial $S_o^l = 0.39$ before freeze-drying and another sample with initial $S_o^l = 0.59$.

These MIP data are extrapolated in the range $D < 6.8\text{nm}$ to estimate the size distribution of the pores that are not intruded by mercury. The extrapolated part is assumed to smoothly follow the trend of the MIP data and is constructed manually, with the only purpose to clarify

the proposed method idea. In real cases, however, a suitable mathematical probability distribution function that fits the MIP data would be advisable to be used instead.

With reference to Table 1, the following paragraphs discuss in details the implementation of each step in the current example.

Estimation of predicted degree of saturation by MIP measurements (S_{MIP})

The measured curves of the intruded mercury void ratio versus pore radius, as given in Delage *et al.* (2006) are converted to the curves of S_{MIP} versus suction by employing Equations (12) and (13). The results are shown in Fig. 9. These curves are later used to estimate the interparticle saturation S_{out} .

Estimation of contribution of interlayer saturation, interlayer void ratio and the scaling factor (S_{int} , e_{int} and α)

By examining the data in Fig. 3 related to the interlayer distance evolution with suction, and the physical properties of MX-80 bentonite as listed in Table 2, Equation (7) and Equation (2) predict the contribution of the interlayer water to the total degree of saturation as represented by the blue dashed curve in Fig. 10. This curve corresponds to the minimum degree of saturation that should be available in the soil sample at any suction level. Equations (9) and (14) are then used to estimate e_{int} and consequently the scaling factor α to be applied on S_{MIP} . The scaling factor varies with suction as, for instance, given in Fig. 10 for $e_o = 0.648$ and $S_o^l = 0.59$. Similar procedure applies for the MIP data of the sample with $S_o^l = 0.39$ and $e_o = 0.649$ which gives different S_{MIP} and α curves.

Estimation of the contribution of interparticle saturation based on MIP data

Following the algorithm in Table 1, the calculated S_{MIP} data is scaled down by factor α to get the contribution of interparticle saturation S_{out} . This contribution is then added to the interlayer contribution S_{int} to get the total degree of saturation estimation S^l as shown in Fig.

11. This total degree of saturation curve is only valid at the corresponding initial degree of saturation of the MIP sample. For the given initial degree of saturation of $S^l = 0.59$, only the point shown as a red square mark in Fig. 11 is valid and corresponds to suction $s = 42000\text{kPa}$. It represents the first estimated point on the targeted SWCC. Upon repeating exactly the same procedure for the sample with $S_o^l = 0.39$, one ends up with the second point on the SWCC with the coordinates ($s = 80000\text{kPa}$, $S^l = 0.39$). The used data in this case are depicted in Fig. 12.

Predicted versus measured soil water characteristic curve

These two MIP tests at different initial degree of saturation, following the proposed method, yielded two points of the SWCC. Now, one might use two additional points at the boundaries assuming that at $s = 1.0\text{kPa}$ the total degree of saturation is 1.0 and at very high suction $s = 10^6\text{kPa}$ the degree of saturation is 0.0 (Fredlund & Xing, 1994; Romero *et al.*, 2011). Having these four points, any suitable fitting model can be employed to build the full SWCC. For example, Fig. 13 shows the fitting result upon employing the well-known van Genuchten model (van Genuchten, 1980):

$$S^l = (S_{sat}^l - S_{res}^l)[1 + (g_\alpha s)^{g_n}]^{g_m} + S_{res}^l \quad (16)$$

where g_α , g_n and g_m are fitting parameters. The symbols S_{sat}^l and S_{res}^l denote the degree of saturation at full saturation and at the residual state. In these validation examples, they are taken equal to 1.0 and 0.0, respectively. Fig. 13 gives the values of all the used fitting parameters.

Fig. 14 shows the measured data of the SWCC by Delage *et al.* (2006) and Villar *et al.* (2005) being plotted on top of Fig. 13. It shows a perfect replication of the soil water characteristic curve measurements, which validates the procedure in this case.

VALIDATION BASED ON DATA FROM Seiphoori *et al.* (2014)

To have an in depth view on the effect of microstructure evolution on the water retention characteristics of MX-80 bentonite, Seiphoori *et al.* (2014) conducted several MIP measurements which demonstrated, among other points, the effect of different hydraulic paths on micro and macro pore size distribution.

The validation here bases only on a single set of measurements. To keep the consistency, the employed physical properties of MX-80 bentonite are the same as in the previous example and listed in Table 2. Seiphoori *et al.* (2014) used WP4 dewpoint potentiometer to obtain the water retention curve for a sample with $\rho_d = 1.8\text{Mg/m}^3$ ($e_o = 0.53$) under constant volume. In the mercury intrusion porosimetry test the maximum applied intrusion mercury pressure was 400MPa which allowed for intrusion of pores with minimum diameter of $D = 4.0\text{nm}$, that is smaller than in previously used data (Delage *et al.*, 2006).

The MIP measurements are provided in terms of accumulated intruded void ratio for three samples, which had similar initial e_o but different initial degrees of saturation before freeze-drying ($S_o^l = 0.28, 0.62$ and 1.0). As in the preceding example, extrapolation is used to cover the non-intruded pore size range ($D < 4.0\text{nm}$).

Based on the proposed algorithm in Table 1, the following paragraphs present the detailed steps to estimate the water retention curve employing the new data.

Estimation of predicted degree of saturation by MIP measurements (S_{MIP})

The MIP data lead to the corresponding degree of saturation with the results depicted in Fig. 15 for the three samples at three different initial degrees of saturation.

Estimation of contribution of interlayer saturation, interlayer void ratio and the scaling factor (S_{int}, e_{int} and α)

The contribution of the interlayer water to the total degree of saturation is estimated by Equation (2). The interlayer void ratio and consequently the scaling factor α come from Equations (9) and (14), respectively. Fig. 16 presents the relevant results for the sample with $S_o^l = 0.28$. It is clear in the figure that at high saturation the interlayer water dominates for the soil sample with such a high dry density ($e_o = 0.53$). In the suction range lower than 1000kPa most of the water is the interlayer water. Same equations lead to the curves for other degrees of saturation (e.g. $S_o^l = 0.62$ and $S_o^l = 1.0$).

Estimation of the contribution of interparticle saturation based on MIP data

The contribution of the interparticle saturation S_{out} is estimated by scaling the calculated S_{MIP} data by the α factor. The resulted value is added to the interlayer contribution S_{int} as estimated in the previous paragraph to get the total degree of saturation S^l . The total degree of saturation curve is only valid at the corresponding initial degree of saturation of the MIP sample. Fig. 17, Fig. 18 and Fig. 19 graphically illustrate the procedure for the three samples with different initial degrees of saturation $S_o^l = 0.28$, $S_o^l = 0.62$ and $S_o^l = 1.0$, respectively. As it is clear in the figures, these three samples yield three different points on the SWCC with the coordinates ($s = 140000\text{kPa}$, $S^l = 0.28$), ($s = 70000\text{kPa}$, $S^l = 0.62$) and ($s = 2000\text{kPa}$, $S^l = 1.0$).

Predicted versus measured soil water characteristic curve

Following a similar procedure to that in Delage *et al.* (2006) example, to the three estimated points, one might add two additional points at the boundaries with the coordinates ($s = 1\text{kPa}$, $S^l = 1.0$) and ($s = 10^6\text{kPa}$, $S^l = 0.0$). These five points are fitted with the van Genuchten model as shown in Fig. 20, which also gives the model fitting parameters values.

Examination of the measured SWCC data and the obtained water retention curve in Fig. 21 reveals an excellent match and further confirms the validity of the proposed method.

VALIDATION IN CASE OF GAOMIAOZI (GMZ) BENTONITE

Gaomiaozi (GMZ) bentonite, the main candidate as a nuclear waste sealing material in China, has received detailed experimental characterisation and its physical properties are well established (Ye *et al.*, 2010, 2012, 2014a, 2014b; Chen *et al.*, 2017; Xu, Ye & Ye, 2017).

Table 3 lists the most relevant physical properties to this validation example.

Ye *et al.* (2010) and Xu *et al.* (2017) reported measurements of the water retention curve at dry density $\rho_d = 1.7\text{Mg/m}^3$ ($e_o = 0.564$) using the vapour equilibrium technique. For the same dry density, Ye *et al.* (2009) and Lui (2016) provided MIP data for compacted GMZ bentonite at different initial degree of saturation.

Ye *et al.* (2009) gave MIP curve at the initial suction value of $s_o = 1000\text{kPa}$ without mentioning the corresponding water content in the original work. Nonetheless, the value of initial suction is equally useful for the proposed procedure.

Adopting the algorithm in Table 1, the following steps clarify how to estimate the water retention curve for GMZ bentonite.

Estimation of predicted degree of saturation by MIP measurements (S_{MIP})

Lui (2016) provided the MIP data at $S_o^l = 0.51$ and 0.63 as pore size density curves being defined as $\text{PSD} = \frac{\Delta V_{in}}{\Delta \log D}$ versus the pore diameter D . Correspondingly, the increment of

intruded pore volume $\Delta V_{in,i}$ at the related i^{th} average pore diameter D_i , computed as average between the diameters at the beginning and the end of the pore diameter increment ΔD_i equals:

$$\Delta V_{in,i} = \frac{\Delta D_i}{D_i \ln(10)} \text{PSD}_i \quad (17)$$

Consequently, the accumulated intruded void volume $V_{in,i}$ per unit mass and the intruded void ratio $e_{in,i}$ at the average pore diameter D_i are:

$$V_{in,i} = \sum_{k=1}^i \Delta V_{in,k}; \quad e_{in,i} = \rho_s V_{in,i} \quad (18)$$

where $k = 1$ to i . Using Equations (17) and (18), the authors converted the provided pore size density curves back to the accumulated intruded void ratio curves. Based on these curves, the estimated degree of saturation by MIP data are estimated and depicted in Fig. 22.

Estimation of contribution of interlayer saturation, interlayer void ratio and the scaling factor (S_{int} , e_{int} and α)

The interlayer water contribution to the total degree of saturation S_{int} , the interlayer void ratio e_{int} and the scaling factor α are estimated by Equation (2), (9) and (14), respectively.

The interlayer water content w_{int} in Equation (2) is determined through Equation (7). The result in case of the sample with initial degree of saturation $S_o^l = 0.63$ is depicted in Fig. 23.

Similar procedure applies for the other two samples.

Estimation of the contribution of interparticle saturation based on MIP data

To estimate the contribution of the interparticle saturation S_{out} , the calculated S_{MIP} data are scaled by the factor α . Subsequently, the S_{out} value is added to the previously estimated interlayer contribution S_{int} to obtain the total degree of saturation S^l which is only valid at the corresponding initial degree of saturation of the MIP sample. The results for the three tested samples are shown in Fig. 24, Fig. 25 and Fig. 26 with $S_o^l = 0.63$, $S_o^l = 0.51$ and $s_o = 1000\text{kPa}$, respectively. The procedure predicts that the points ($s = 64000\text{kPa}$, $S^l = 0.51$), ($s = 46500\text{kPa}$, $S^l = 0.63$) and ($s = 1000\text{kPa}$, $S^l = 0.97$) to be on the retention curve of the compacted GMZ bentonite with dry density $\rho_d = 1.7\text{Mg/m}^3$. It is worth noting that the given initial suction in the sample in Fig. 26 is used to estimate the initial degree of saturation, unlike as in the two other samples with given initial degree of saturation.

Predicted versus measured soil water characteristic curve

Again, in addition to the three predicted points, one could add two additional points at the boundaries with the coordinates ($s = 1\text{kPa}$, $S^l = 1.0$) and ($s = 10^6\text{kPa}$, $S^l = 0.0$). Fig. 27 shows the fitting result of these points with the corresponding fitting parameters values. The measured SWCC data validates the procedure for GMZ bentonite as illustrated in Fig. 28. Upon examining Fig. 28, it seems that the predicted points fit the experimental curve very well, though the van Genuchten fit would be improved by having the two defining point of the curve further apart, or assuming a higher value of suction at zero degree of saturation.

CONCLUSIONS

The paper proposes a new procedure to estimate the soil water characteristic curve for bentonite based on mineralogy, simple physical properties and MIP measurements. The main assumption is that at any total suction value, the available water in the geomaterial can be decomposed to the interlayer water, which exists in between clay unit layers and the interparticle water that resides everywhere else in the available pores. A simplified formula is introduced to estimate the interlayer water content. The formula requires the knowledge of the material specific surface and the weight ratio of the composing minerals.

The interparticle water content is estimated based on the MIP measurements. To account for the effect of freeze-drying on the microstructure of the bentonite, a factor is introduced to scale down the available pore for the intrusion. The factor is a function of interlayer void ratio and evolves with saturation. The proposed framework is validated against available data in literature and proved to replicate the experiments very well.

Despite the focus on bentonite, the procedure may be more generic and perhaps be used for any geomaterial. The framework allows for an indirect estimation of the water retention properties of the material based on the mercury intrusion porosimetry (MIP) measurements,

which may lead to time savings and provides an elegant modelling tool for the estimation of SWCC under different hydro-mechanical paths.

ACKNOWLEDGEMENT

The authors would like to gratefully acknowledge that the presented research has been funded by KYT2018 Finnish Research Programme on Nuclear Waste Management via THEBES project.

NOTATION

Roman

A	Fitting parameter, L	S_{int}	Contribution due to interlayer spaces saturation
A_l	Clay layer surface area, L ²		
B	Fitting parameter, M ⁻¹ L T ²	S_{MIP}	Predicted degree of saturation by MIP measurements
C	Auxiliary term	S_{out}	Contribution due to interparticle pores saturation
D	Pore diameter, L	S_s	Specific surface, L ² M ⁻¹
e_o	Initial void ratio	V_{in}	Mercury intruded pore volume per unit mass, L ³ M ⁻¹
e_{in}	Mercury intruded void ratio	V_s	Solid particles volume per unit mass, L ³ M ⁻¹
e_{int}	Interlayer void ratio	V_v	Voids volume per unit mass, L ³ M ⁻¹
e_{out}	Interparticle void ratio	w	Water content
g_a	van Genuchten fitting parameter	w_{int}	Interlayer water content
g_m	van Genuchten fitting parameter	w_L	Liquid limit
g_n	van Genuchten fitting parameter	w_p	Plastic limit
G_s	Specific gravity	w_{sat}	Saturated water content
I_p	Plasticity index		
L	Number of clay layers per particle	<i>Greek</i>	
m	Number of water layers in between two adjacent clay layers	α	Scaling factor
n	Number of water layers on the outer surface of a clay particle	α_c	The contact angle between the fluid and the soil particle
NA	Total number of clay particles per unit mass, M ⁻¹	δ_{int}	Interlayer spacing, L
R_i	The percentage of the composing mineralogy by weight of total solids	δ_w	The thickness of one water layer, L
s	Total suction, M L ⁻¹ T ⁻²	ρ_d	Dry density, M L ⁻³
s_o	Total initial suction before freeze-drying, M L ⁻¹ T ⁻²	ρ_s	Solid particles density, M L ⁻³
S^l	Total degree of saturation	ρ_w	Free water density, M L ⁻³
S_o^l	Initial total degree of saturation	ρ_w^{int}	Interparticle water density, M L ⁻³
S_{in}	Mercury degree of saturation	σ^t	Surface tension of water, M T ⁻²

Abbreviations

MIP	Mercury Intrusion Porosimetry
SWCC	Soil Water Characteristic Curve
THMC	Thermo-Hydro-Mechanical-Chemical

Note: Units are given after the comma; where L, M and T mean units of length, mass and time, respectively.

REFERENCES

- Abed, A.A. & Sołowski, W.T. (2017). A study on how to couple thermo-hydro-mechanical behaviour of unsaturated soils: Physical equations, numerical implementation and examples. *Computers and Geotechnics* **92**, 132–155.
- ASTM, D. (1998). 4404 “Standard test method for determination of pore volume and pore volume distribution of soil and rock by mercury intrusion porosimetry”. *ASTM International*.
- Bergaya, F. & Lagaly, G. (2013) *Handbook of Clay Science*. Newnes.
- Bestel, M., Diamond, L.W., Glaus, M.A., Gimmi, T., Van Loon, L.R. & Jurányi, L. (2014). *Water–montmorillonite systems: Neutron scattering and tracer through diffusion studies*. PhD thesis, Universität Bern, Bern, Switzerland.
- Branson, K. & Newman, A.C.D. (1983). Water sorption on Ca-saturated clays: I. Multilayer sorption and microporosity in some illites. *Clay Minerals* **18**, No. 3, 277-287.
- Bucher, F. & Müller-Vonmoos, M. (1989). Bentonite as a containment barrier for the disposal of highly radioactive wastes. *Applied Clay Science* **4**, No. 2, 157–177.
- Chen, Z.G., Tang, C.S., Shen, Z., Liu, Y.M. & Shi, B. (2017). The geotechnical properties of GMZ buffer/backfill material used in high-level radioactive nuclear waste geological repository: a review. *Environmental Earth Sciences* **76**, No. 7, p. 270.
- Chipera, S.J., Carey, J.W. & Bish, D.L. (1998). Controlled-humidity XRD analyses: Application to the study of smectite expansion/contraction. In: *Advances in X-ray Analysis*. Springer. pp. 713–722.
- Collin, F., Li, X.L., Radu, J.P. & Charlier, R. (2002). Thermo-hydro-mechanical coupling in clay barriers. *Engineering Geology* **64**, No. 2, 179–193.
- Deirieh, A., Chang, I.Y., Whittaker, M.L., Weigand, S., Keane, D., Rix, J., Germaine, J.T., Joester, D. & Flemings, P.B. (2018). Particle arrangements in clay slurries: The case against the honeycomb structure. *Applied Clay Science*, **152**, 166-172.
- Delage, P. & Lefebvre, G. (1984). Study of the structure of a sensitive Champlain clay and of its evolution during consolidation. *Canadian Geotechnical Journal* **21**, No. 1, 21–35.
- Delage, P., Howat, M.D. & Cui, Y.J. (1998). The relationship between suction and swelling properties in a heavily compacted unsaturated clay. *Engineering geology* **50**, No.1-2, 31-48.
- Delage, P., Marcial, D., Cui, Y.J. & Ruiz, X. (2006). Ageing effects in a compacted bentonite: a microstructure approach. *Géotechnique* **56**, No. 5, 291–304.
- Della Vecchia, G., Dieudonné, A., Jommi, C. & Charlier, R. (2015). Accounting for evolving pore size distribution in water retention models for compacted clays. *International Journal for Numerical and Analytical Methods in Geomechanics* **39**, No. 7, 702–723.

- Fredlund, D.G. & Rahardjo, H. (1993). *Soil mechanics for unsaturated soils*. John Wiley & Sons.
- Fredlund, D.G. & Xing, A. (1994). Equations for the soil-water characteristic curve. *Canadian geotechnical journal* **31**, No. 4, 521–532.
- Gallé, C. (2001). Effect of drying on cement-based materials pore structure as identified by mercury intrusion porosimetry: a comparative study between oven-, vacuum-, and freeze-drying. *Cement and Concrete Research* **31**, No. 10, 1467–1477.
- Gens, A. & Alonso, E.E. (1992). A framework for the behaviour of unsaturated expansive clays. *Canadian Geotechnical Journal* **29**, No. 6, 1013–1032.
- Greene-Kelly, R. (1973). The preparation of clay soils for determination of structure. *Journal of Soil Science* **24**, No. 3, 277–283.
- Haines, W.B. (1930). Studies in the physical properties of soil. V. The hysteresis effect in capillary properties, and the modes of moisture distribution associated therewith. *The Journal of Agricultural Science* **20**, No. 1, 97–116.
- Holtz, R.D. & Kovacs, W.D. (1981). *An introduction to geotechnical engineering*. Englewood Cliffs, NJ: Prentice-Hall.
- Hsiao, Y.-W. & Hedström, M. (2017). Swelling Pressure in Systems with Na-Montmorillonite and Neutral Surfaces: A Molecular Dynamics Study. *The Journal of Physical Chemistry C*. [Online] **121**, No. 47, 26414–26423. Available from: doi:10.1021/acs.jpcc.7b09496.
- Jacinto, A.C., Villar, M.V., Gómez-Espina, R. & Ledesma, A. (2009). Adaptation of the van Genuchten expression to the effects of temperature and density for compacted bentonites. *Applied Clay Science* **42**, No. 3, 575–582.
- Jacinto, A.C., Villar, M.V. & Ledesma, A. (2012). Influence of water density on the water-retention curve of expansive clays. *Geotechnique* **62**, No. 8, 657–667.
- Kraehenbuehl, F., Stoeckli, H.F., Brunner, F., Kahr, G. & Müller-Vonmoos, M. (1987). Study of the water-bentonite system by vapour adsorption, immersion calorimetry and X-ray techniques: I. Micropore volumes and internal surface areas, following Dubinin's theory. *Clay Minerals* **22**, No. 1, 1-9.
- Kuusela-Lahtinen, A., Sinnathamby, G., Mendez, J., Sołowski, W.T., Gallipoli, D., Pintado, X. & Korkiala-Tanttu, L.K. (2016). Estimation of water retention behaviour of MX-80 bentonite partially saturated with saline solution. In: *E3S Web of Conferences*. 2016 EDP Sciences. p. 11006.
- Lawrence, G.P. (1978). Stability of soil pores during mercury intrusion porosimetry. *European Journal of Soil Science* **29**, No. 3, 299–304.

- Lawrence, G.P., Payne, D. & Greenland, D.J. (1979). Pore size distribution in critical point and freeze dried aggregates from clay subsoils. *Journal of soil science* **30**, No. 3, 499–516.
- Leong, E.C. & Rahardjo, H. (1997). Review of soil-water characteristic curve equations. *Journal of Geotechnical and Geoenvironmental Engineering* **123**, No. 12, 1106–1117.
- Likos, W.J. & Wayllace, A. (2010). Porosity evolution of free and confined bentonites during interlayer hydration. *Clays and Clay minerals* **58**, No. 3, 399–414.
- Lourenço, S.D.N., Gallipoli, D., Augarde, C.E., Toll, D.G., et al. (2012). Formation and evolution of water menisci in unsaturated granular media. *Géotechnique* **62**, No. 3, 193–199.
- Lui, Y. (2016). Investigation on the swelling properties and microstructure mechanism of compacted Gaomiaozhi bentonite. *Journal of Engineering Geology* **24**, No. 3, 451–458.
- Marcial, D. (2011). A simple method to consider water density changes in the calculation of the degree of saturation of swelling clays. *Unsaturated Soils. CRC Press/Balkema, London*. 473–478.
- Marinho, F.A. (2005) Nature of soil–water characteristic curve for plastic soils. *Journal of Geotechnical and Geoenvironmental Engineering* **131**, No. 5, 654–661.
- Monroy, R., Zdravkovic, L. & Ridley, A. (2010). Evolution of microstructure in compacted London Clay during wetting and loading. *Géotechnique* **60**, No. 2, 105–119.
- Murray, R.S. & Quirk, J.P. (1980). Freeze-Dried and Critical-Point-Dried Clay—A Comparison. *Soil Science Society of America Journal* **44**, No. 2, 232–234.
- Musso, G., Romero, E. & Della Vecchia, G. (2013). Double-structure effects on the chemo-hydro-mechanical behaviour of a compacted active clay. *Géotechnique* **63**, No. 3, 206–220.
- Nowamooz, H. & Masrouri, F. (2010). Relationships between soil fabric and suction cycles in compacted swelling soils. *Engineering Geology* **114**, No. 3–4, 444–455.
- Olivella, S., Gens, A., Carrera, J. & Alonso, E.E. (1996). Numerical formulation for a simulator (CODE_BRIGHT) for the coupled analysis of saline media. *Engineering Computations* **13**, No. 7, 87–112.
- Prapaharan, S., Altschaeffl, A.G. & Dempsey, B.J. (1985). Moisture curve of compacted clay: mercury intrusion method. *Journal of Geotechnical Engineering* **111**, No. 9, 1139–1143.
- Pusch, R. (2015). *Bentonite clay: environmental properties and applications*. CRC Press.
- Ritter, H.L. & Erich, L.C. (1948). Pore size distribution in porous materials. *Analytical Chemistry* **20**, No. 7, 665–670.

- Romero, E., Della Vecchia, G. & Jommi, C. (2011). An insight into the water retention properties of compacted clayey soils. *Géotechnique* **61**, No. 4, 313–328.
- Romero, E., Gens, A. & Lloret, A. (1999). Water permeability, water retention and microstructure of unsaturated compacted Boom clay. *Engineering Geology* **54**, No. 1–2, 117–127.
- Romero, E. & Simms, P.H. (2008). Microstructure investigation in unsaturated soils: a review with special attention to contribution of mercury intrusion porosimetry and environmental scanning electron microscopy. *Geotechnical and Geological Engineering* **26**, No. 6, 705–727.
- Romero, E. (1999). *Characterisation and thermo-hydro-mechanical behaviour of unsaturated Boom clay: an experimental study*. PhD thesis, Universitat Politècnica de Catalunya, Barcelona, Spain.
- Saiyouri, N., Hicher, P.Y. & Tessier, D. (2000). Microstructural approach and transfer water modelling in highly compacted unsaturated swelling clays. *Mechanics of Cohesive-Frictional Materials* **5**, No. 1, 41–60.
- Saranya, N. & Arnepalli, D.N. (2018). Effect of drying technique on pore structure characteristics of fine-grained geomaterials. *International Journal of Geotechnical Engineering* **12**, No. 6, 578–591.
- Seiphoori, A., Ferrari, A. & Laloui, L. (2014). Water retention behaviour and microstructural evolution of MX-80 bentonite during wetting and drying cycles. *Géotechnique* **64**, No. 9, 721–734.
- Sellin, P. & Leupin, O.X. (2013). The use of clay as an engineered barrier in radioactive-waste management—a review. *Clays and Clay Minerals* **61**, No. 6, 477–498.
- Sills, I.D., Aylmore, L.A.G. & Quirk, J.P. (1973). A Comparison Between Mercury Injection and Nitrogen Sorption as Methods of Determining Pore Size Distributions. *Soil Science Society of America Journal* **37**, No. 4, 535–537.
- Simms, P.H. & Yanful, E.K. (2002). Predicting soil—water characteristic curves of compacted plastic soils from measured pore-size distributions. *Géotechnique* **52**, No. 4, 269–278.
- Simms, P.H. & Yanful, E.K. (2004). A discussion of the application of mercury intrusion porosimetry for the investigation of soils, including an evaluation of its use to estimate volume change in compacted clayey soils. *Géotechnique* **54**, No. 6, 421–426.
- Tarantino, A. (2009). A water retention model for deformable soils. *Géotechnique* **59**, No. 9, 751–762.
- Thomas, H.R. & He, Y. (1997). A coupled heat-moisture transfer theory for deformable unsaturated soil and its algorithmic implementation. *International Journal for Numerical Methods in Engineering* **40**, No. 18, 3421–3441.

- Tournassat, C. & Appelo, C.A.J. (2011). Modelling approaches for anion-exclusion in compacted Na-bentonite. *Geochimica et Cosmochimica Acta* **75**, No. 13, 3698–3710.
- Tovey, N.K. (1971). Discussion on Session 1: Roscoe Memorial Symposium, Stress-Strain Behavior of Soils. *Proc., Cambridge*. 116–120.
- van Genuchten, M. T. (1980). A closed-form equation for predicting the hydraulic conductivity of unsaturated soils. *Soil Science Society of America Journal* **44**, No. 5, 892–898.
- Villar, M.V. (2005). *MX-80 bentonite, thermo-hydro-mechanical characterisation performed at CIEMAT in the context of the prototype project*. No. Ciemat: 1053, Centro de Investigaciones Energeticas, Madrid, Spain.
- Villar, M.V., Gómez-Espina, R. & Gutiérrez-Nebot, L. (2012). Basal spacings of smectite in compacted bentonite. *Applied Clay Science* **65**, 95–105.
- Washburn, E.W. (1921). Note on a method of determining the distribution of pore sizes in a porous material. *Proceedings of the National Academy of Sciences* **7**, No. 4, 115–116.
- Wierzchoś, J., Ascaso, C., Garcia-Gonzalez, M.T. & Kozak, E. (1992) A new method of dehydration for pure clay materials using Peldri II. *Clays and Clay Minerals* **40**, No. 2, 230–236.
- Wu, W., Li, X., Charlier, R. & Collin, F. (2004). A thermo-hydro-mechanical constitutive model and its numerical modelling for unsaturated soils. *Computers and Geotechnics* **31**, No. 2, 155–167.
- Xu, L., Ye, W.M. & Ye, B. (2017). Gas breakthrough in saturated compacted GaoMiaoZi (GMZ) bentonite under rigid boundary conditions. *Canadian Geotechnical Journal* **54**, No. 8, 1139–1149.
- Ye, W.M., Borrell, N.C., Zhu, J.Y., Chen, B., et al. (2014a). Advances on the investigation of the hydraulic behavior of compacted GMZ bentonite. *Engineering geology* **169**, 41–49.
- Ye, W.M., Chen, Y.G., Chen, B., Wang, Q., et al. (2010). Advances on the knowledge of the buffer/backfill properties of heavily-compacted GMZ bentonite. *Engineering Geology* **116**, No.1–2, 12–20.
- Ye, W.M., Wan, M., Chen, B., Chen, Y.-G., et al. (2012). Temperature effects on the unsaturated permeability of the densely compacted GMZ01 bentonite under confined conditions. *Engineering Geology* **126**, 1–7.
- Ye, W.M., Wang, Q., Chen, Y.G. & Chen, B. (2009). Advances on buffer/backfill properties of heavily compacted Gaomiaozhi bentonite. In: *ISGE2009*, Hangzhou, China.
- Ye, W.M., Zheng, Z.J., Chen, B., Chen, Y.G., Cui, Y.J. & Wang, J. (2014b). Effects of pH and temperature on the swelling pressure and hydraulic conductivity of compacted GMZ01 bentonite. *Applied Clay Science* **101**, 192–198.

Zheng, Y. & Zaoui, A. (2017). Wetting and nanodroplet contact angle of the clay 2: 1 surface: The case of Na-montmorillonite (001). *Applied Surface Science* **396**, 717–722.

Zielinski, M., Sentenac, P., Atique, A., Sánchez, M. & Romero, E.E. (2010). Comparison of four methods for determining the soil water retention curve. In: *Unsaturated soils*. Taylor & Francis. pp. 525–530.

Table captions

Table 1. Steps to follow to locate a point on the water retention curve.

Table 2. Physical properties of MX-80 bentonite after Delage *et al.* (2006).

Table 3. Physical properties of GMZ bentonite (Ye *et al.*, 2010).

Table 1. Steps to follow to locate a point on the water retention curve.

Step 1: Estimate S_{MIP} using Equation (12), based on MIP test (see Fig. 7).

Step 2: For each pore diameter D_i (given by MIP measurements in Step 1 where $i = 1, \dots, n$ and n is the total number of measured MIP points):

- a. Estimate suction s_i according to Equation (13).
- b. Estimate S_{int} and e_{int} using Equation (2) and Equation (9), respectively (see Fig. 8). The interlayer water content w_{int} in Equation (7) is determined through Equation (6).
- c. Estimate the scaling factor α employing Equation (14), see Fig. 7.
- d. Use α to scale the S_{MIP} as estimated in Step 1 to determine S_{out} (see Fig. 7).
- e. Calculate and save the total degree of saturation S_i^l at D_i and the corresponding suction s_i using formula (15).

Step 3: Use the calculate data in Step 2 to construct a full $s - S^l$ curve for the given MIP test and mineralogical data (see Fig. 8).

Step 4: As the resulted curve in Step 3 is only valid at the given total degree of saturation before freeze-drying S_o^l , it is used to find the corresponding suction s_o at that degree of saturation. The resulted pair (s_o, S_o^l) represents the estimated point on the targeted SWCC (see Fig. 8).

Table 2. Physical properties of MX-80 bentonite after Delage *et al.* (2006).

Mineralogy	82% Na-Ca smectite
Liquid limit w_L	520%
Plastic limit w_P	46%
Plasticity index I_P	474
Solid particles density ρ_s	2.65Mg/m ³
Specific surface S_s	522 m ² /g

Table 3. Physical properties of GMZ bentonite (Ye *et al.*, 2010).

Mineralogy	75.4% montmorillonite
Liquid limit w_L	313%
Plastic limit w_P	38%
Plasticity index I_P	275%
Solid particles density ρ_s	2.66Mg/m ³
Specific surface S_s	570 m ² /g

Figure captions

Fig. 1. Idealized pore distribution in clay.

Fig. 2. Visualization of items and corresponding symbols that are employed to estimate interlayer water content.

Fig. 3. Measured interlayer distance versus suction in case of MX-80 bentonite.

Fig. 4. Evolution of interlayer water content and porosity as predicted by Equation (6) and Equation (10) with $\rho_d = 1.6\text{Mg/m}^3$.

Fig. 5. Evolution of interlayer and interparticle void ratio with increasing saturation.

Fig. 6. Components of total degree of saturation.

Fig. 7. Scaling of MIP results to account for interlayer void ratio increase with saturation.

Fig. 8. Graphical illustration of the followed steps in Table 1 to locate a point on the water retention curve.

Fig. 9. Estimated degree of saturation S_{MIP} based on MIP data at two different initial degree of saturation before freeze-drying.

Fig. 10. Contribution of interlayer water and unscaled interparticle water (predicted by MIP) to the total degree of saturation.

Fig. 11. Graphical illustration of the estimation of suction value using mineralogical and MIP data. The sample has an initial degree of saturation of 0.59 before freeze-drying.

Fig. 12. Graphical illustration of the estimation of suction value using mineralogical and MIP data. The sample has an initial degree of saturation of 0.39 before freeze-drying.

Fig. 13. Predicted soil water retention curve for MX-80 bentonite.

Fig. 14. Predicted versus measured soil water retention curve for MX-80 bentonite.

Fig. 15. Estimated degree of saturation S_{MIP} based on MIP data at three different initial degree of saturation before freeze-drying.

Fig. 16. Contribution of interlayer water and unscaled interparticle water (predicted by MIP) to the total degree of saturation.

Fig. 17. Graphical illustration of the estimation of suction value using mineralogical and MIP data. The sample has an initial degree of saturation of 0.28 before freeze-drying.

Fig. 18. Graphical illustration of the estimation of suction value using mineralogical and MIP data. The sample has an initial degree of saturation of 0.62 before freeze-drying.

Fig. 19. Graphical illustration of the estimation of suction value using mineralogical and MIP data. The sample has an initial degree of saturation of 1.0 before freeze-drying.

Fig. 20. Predicted soil water retention curve for MX-80 bentonite.

Fig. 21. Predicted versus measured soil water retention curve for MX-80 bentonite.

Fig. 22. Estimated degree of saturation S_{MIP} based on MIP data at three different initial degree of saturation before freeze-drying.

Fig. 23. Contribution of interlayer water and unscaled interparticle water (predicted by MIP) to the total degree of saturation.

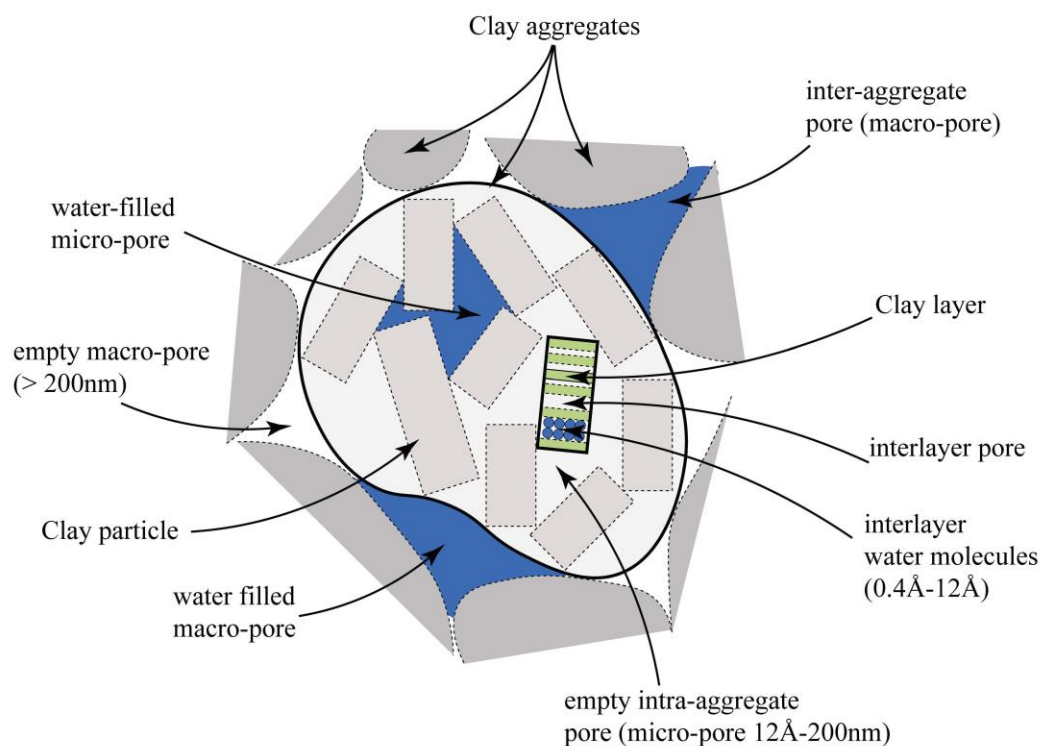
Fig. 24. Graphical illustration of the estimation of suction value using mineralogical and MIP data. The sample has an initial degree of saturation of 0.63 before freeze-drying.

Fig. 25. Graphical illustration of the estimation of suction value using mineralogical and MIP data. The sample has an initial degree of saturation of 0.51 before freeze-drying.

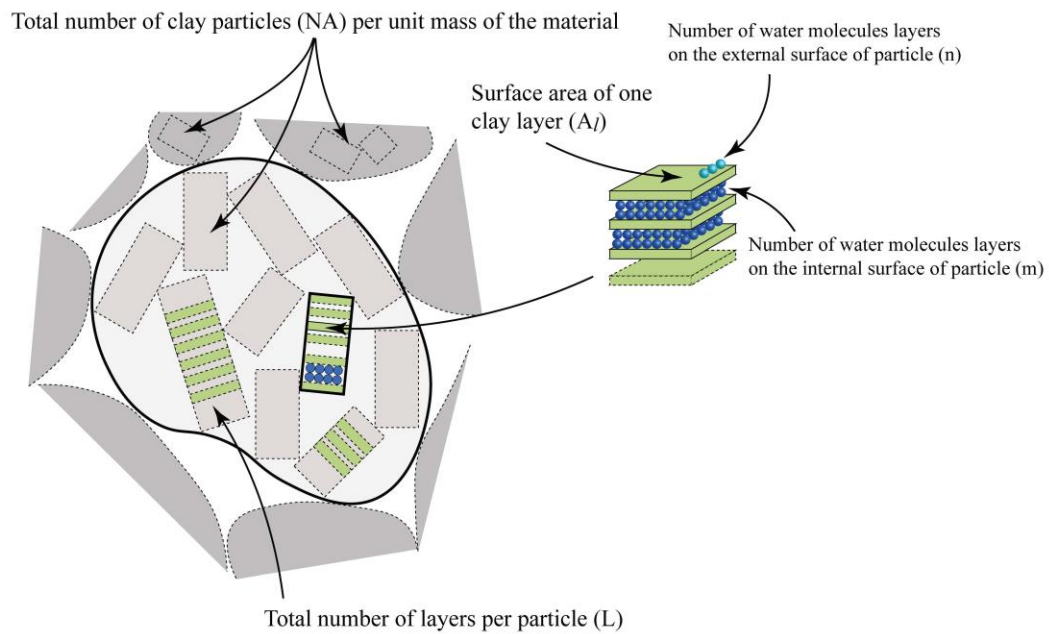
Fig. 26. Graphical illustration of the estimation of initial degree of saturation using mineralogical and MIP data. The sample has an initial suction of 1000kPa before freeze-drying.

Fig. 27. Predicted water retention curve for GMZ bentonite.

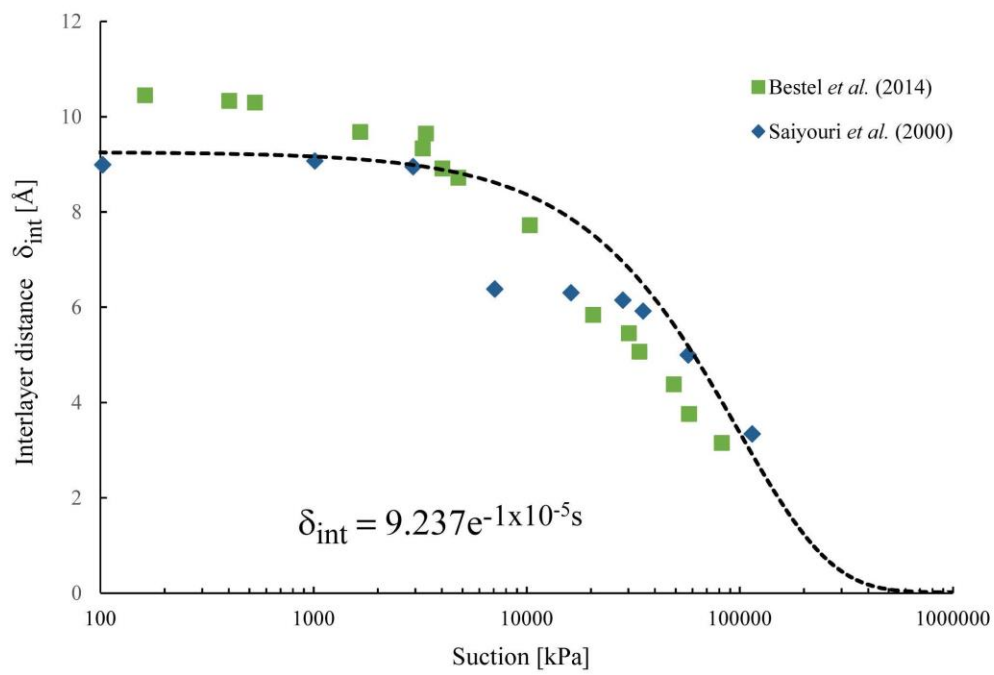
Fig. 28. Predicted versus measured water retention curve for GMZ bentonite.



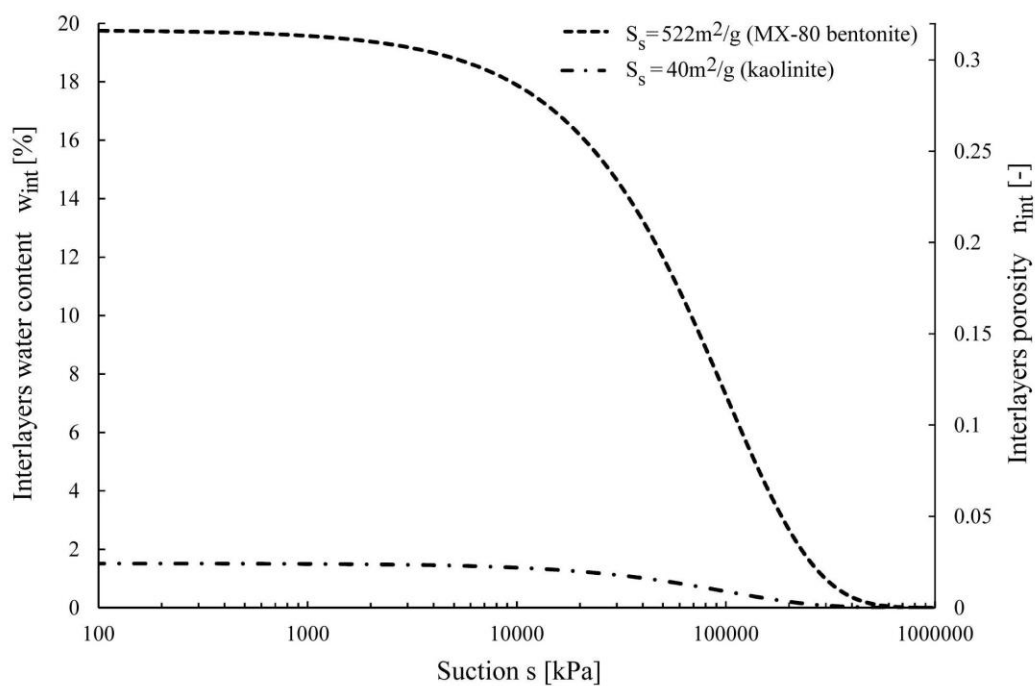
Abedfig1



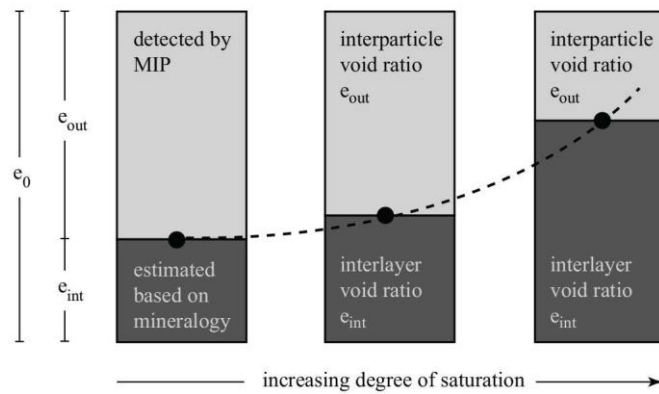
Abefig2



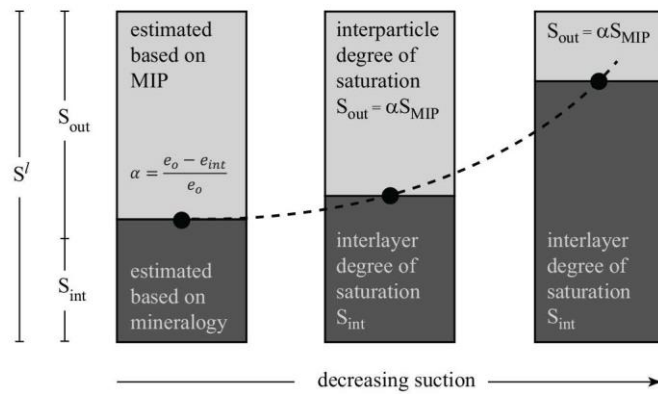
Abedfig3



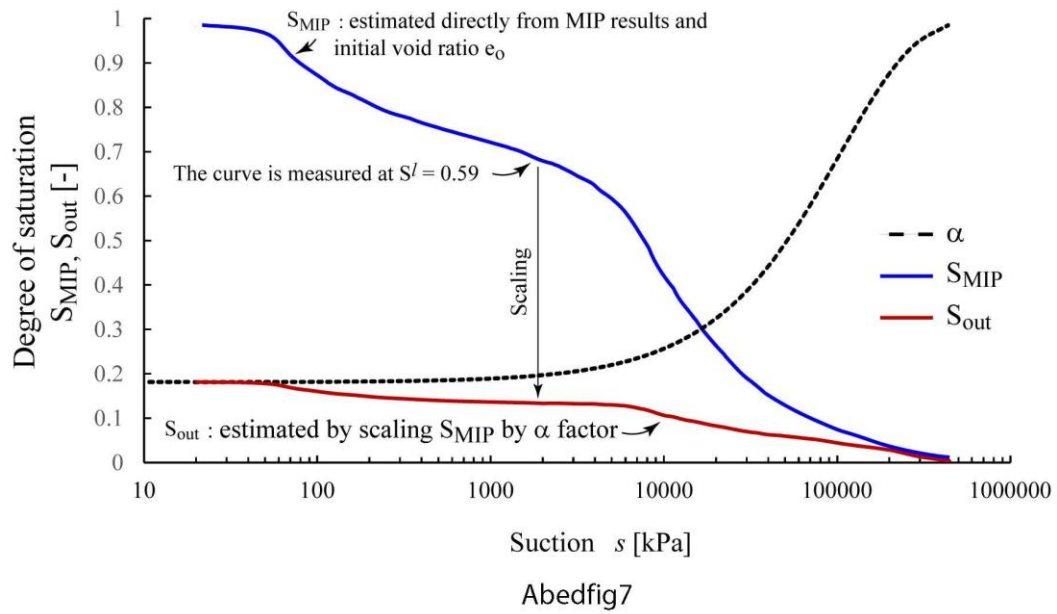
Abedfig4

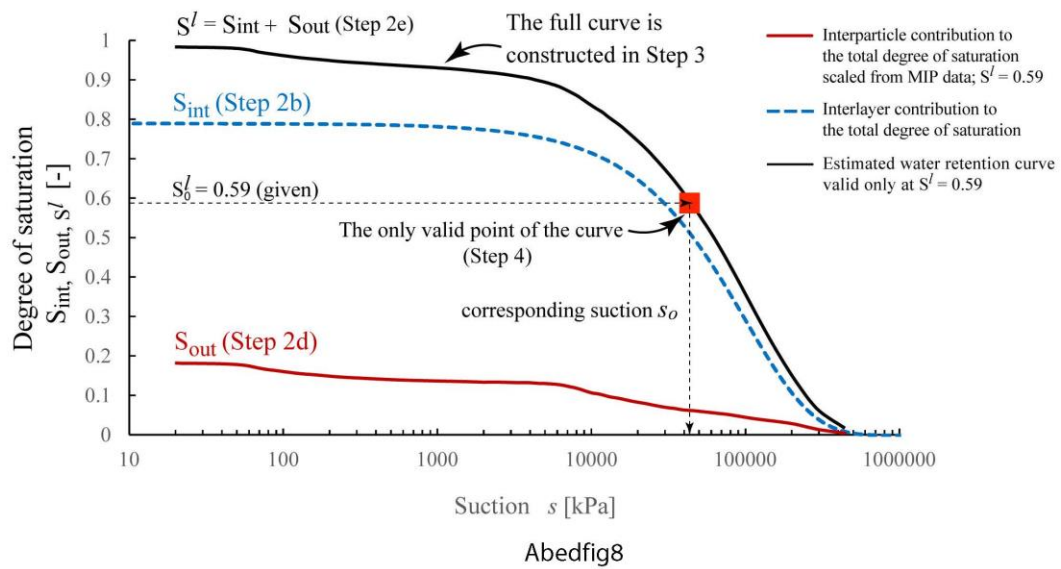


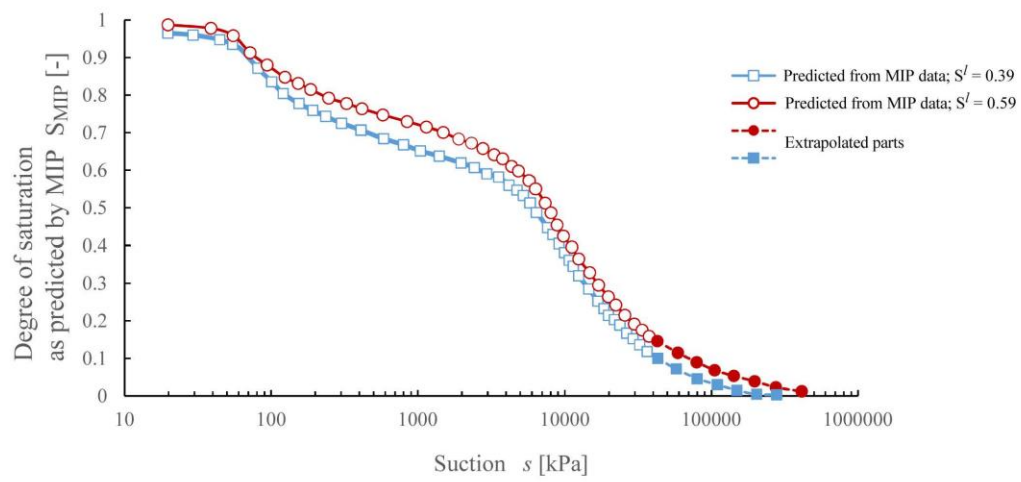
Abedfig5



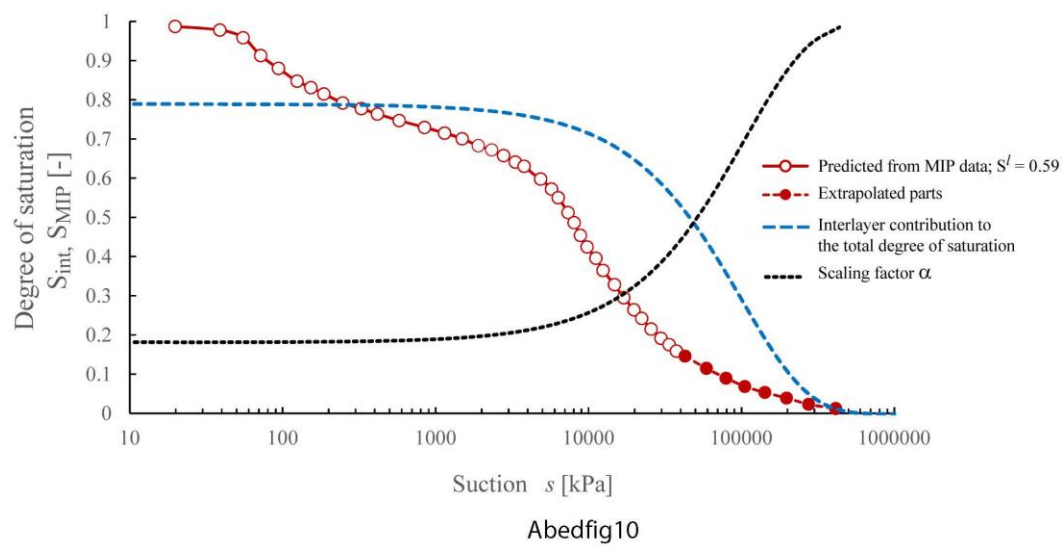
Abedfig6

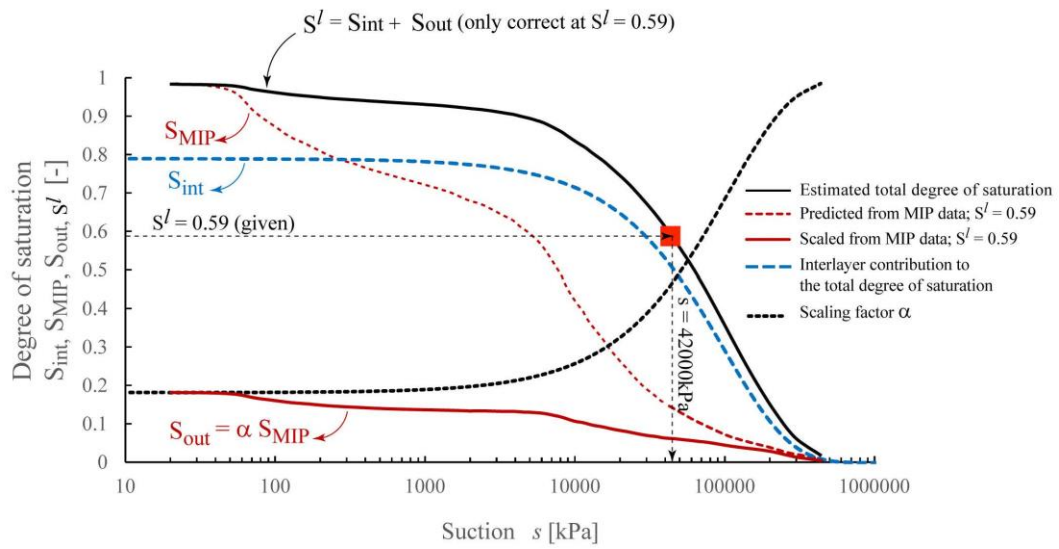




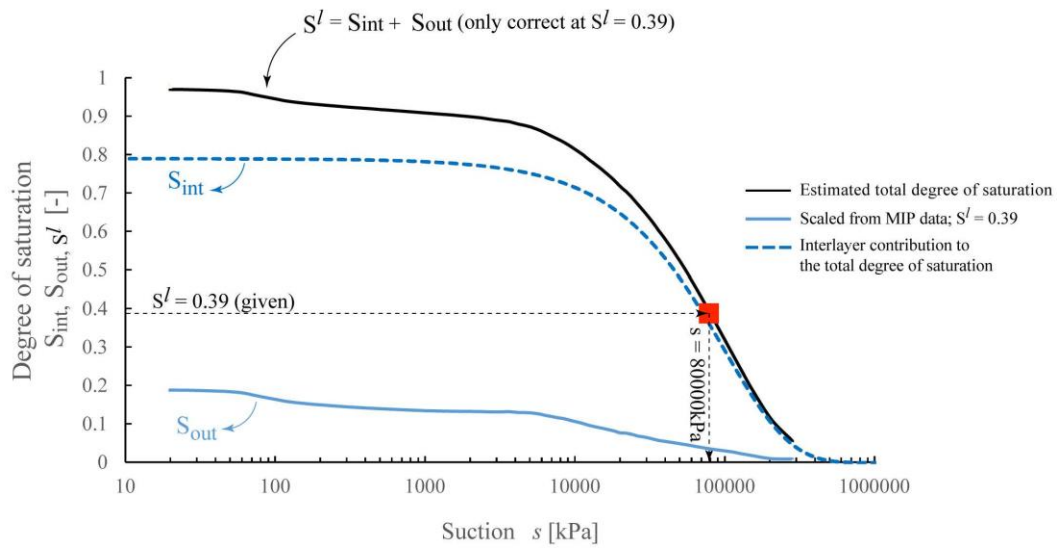


Abedfig9

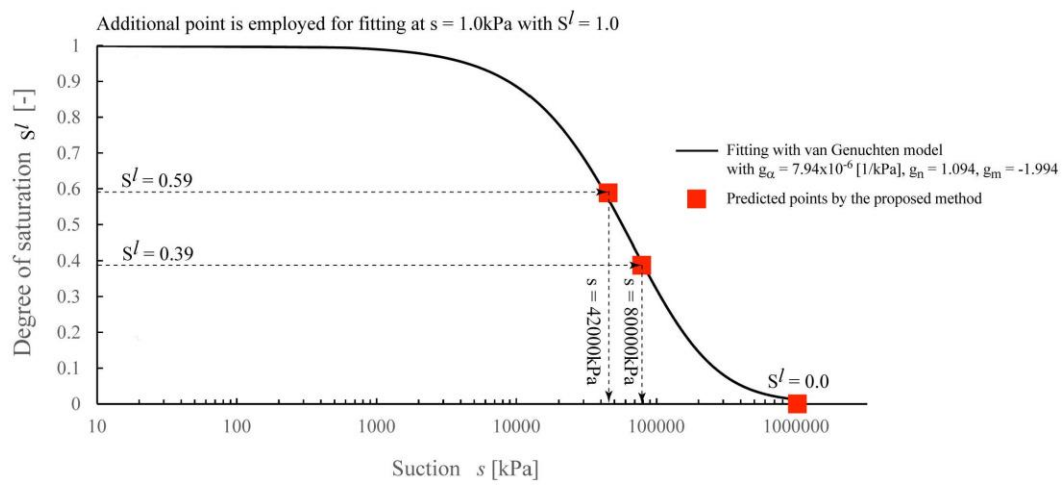




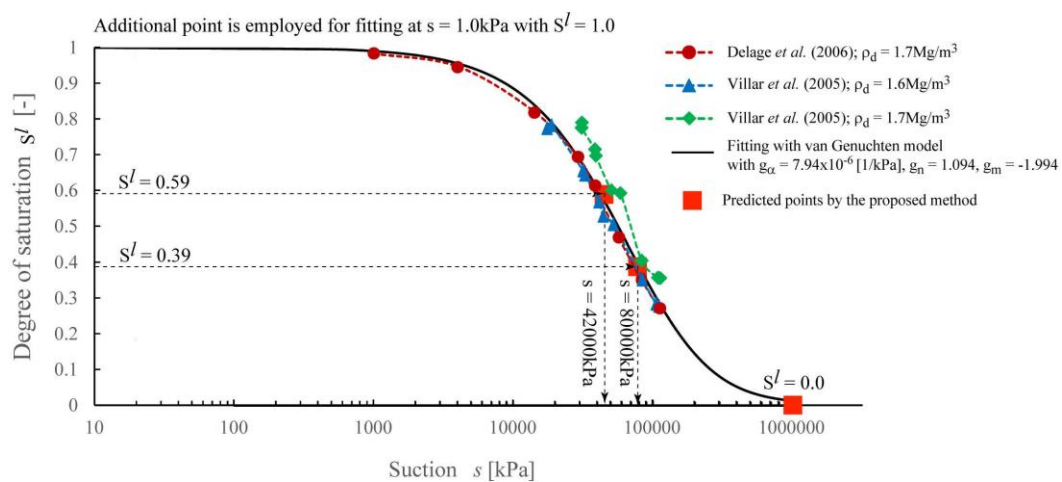
Abedfig11



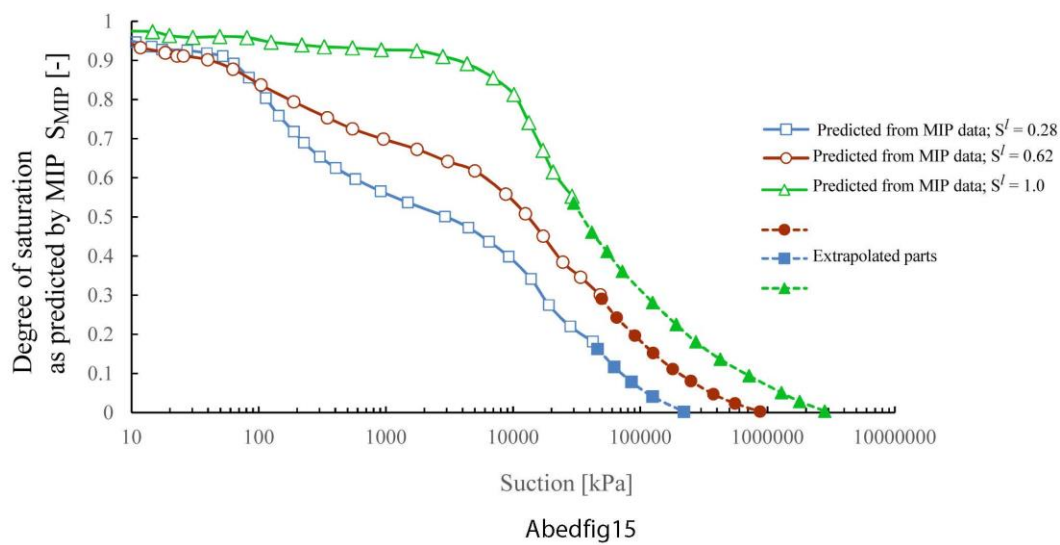
Abedfig12

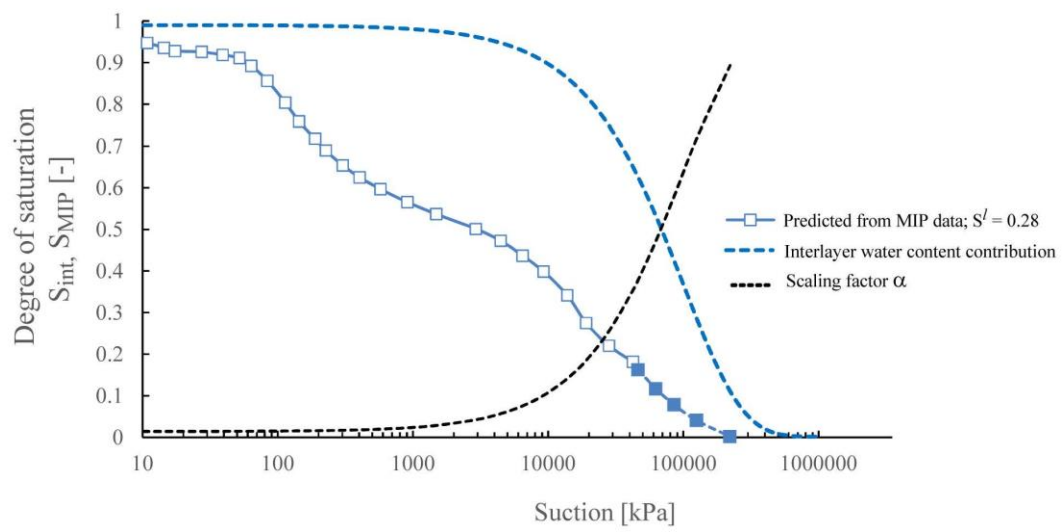


Abedfig13

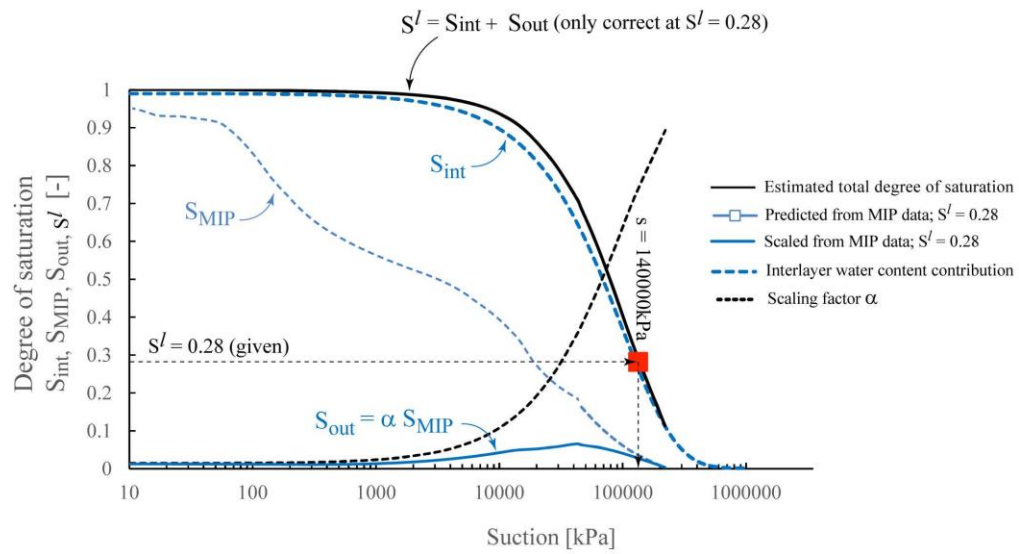


Abedfig14

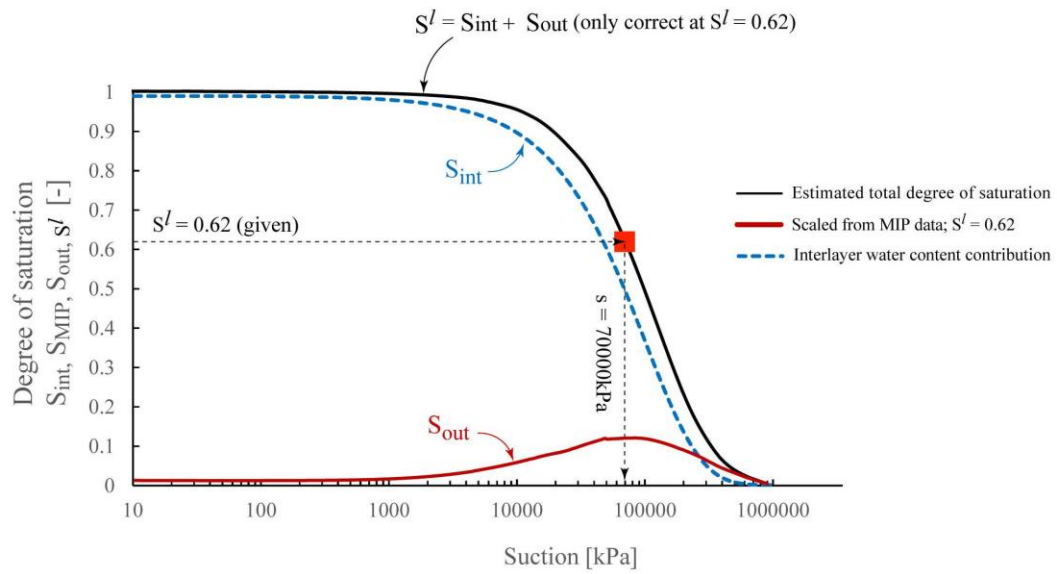




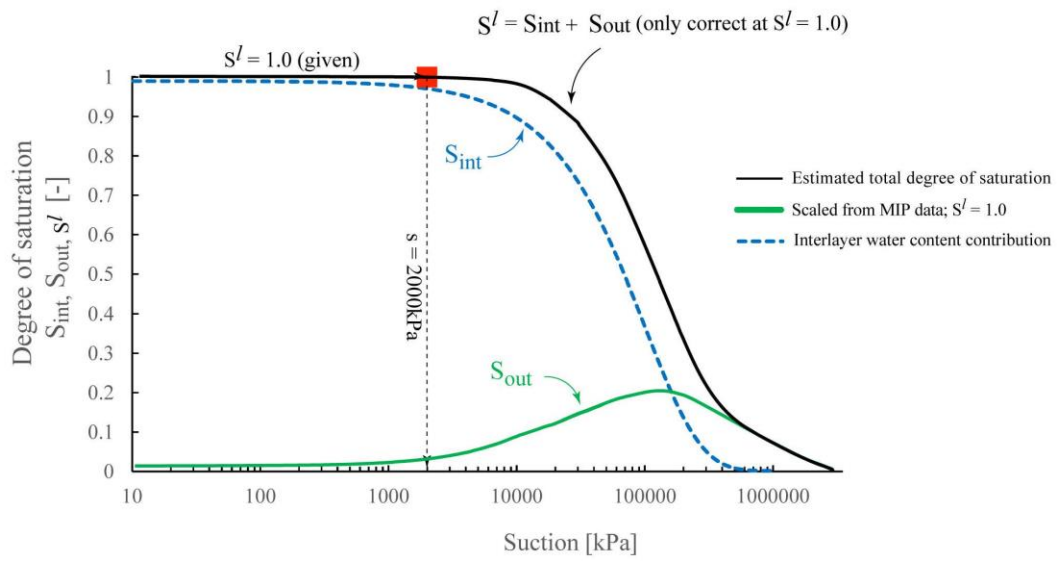
Abedfig16

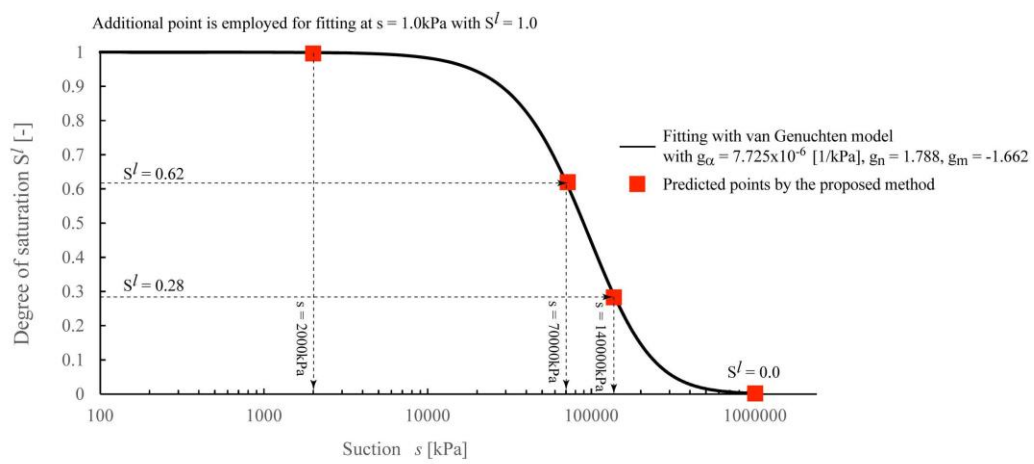


Abedfig17

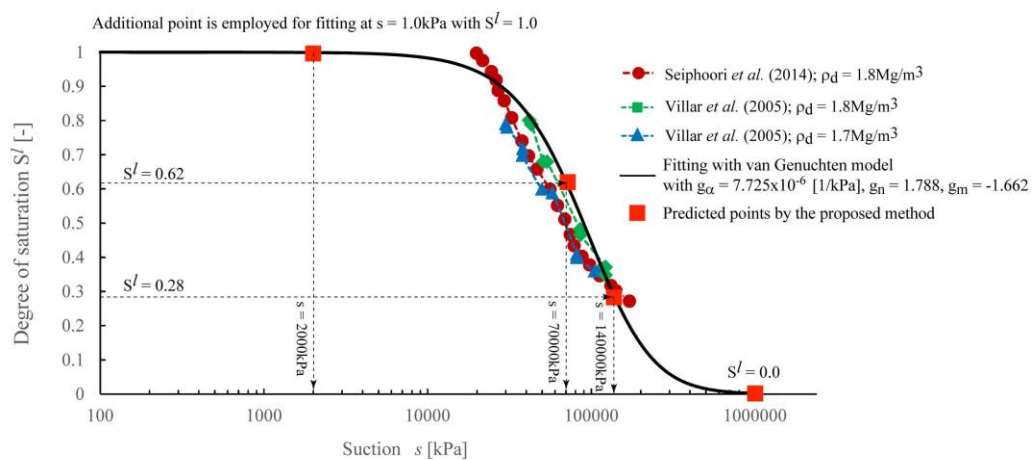


Abedfig18

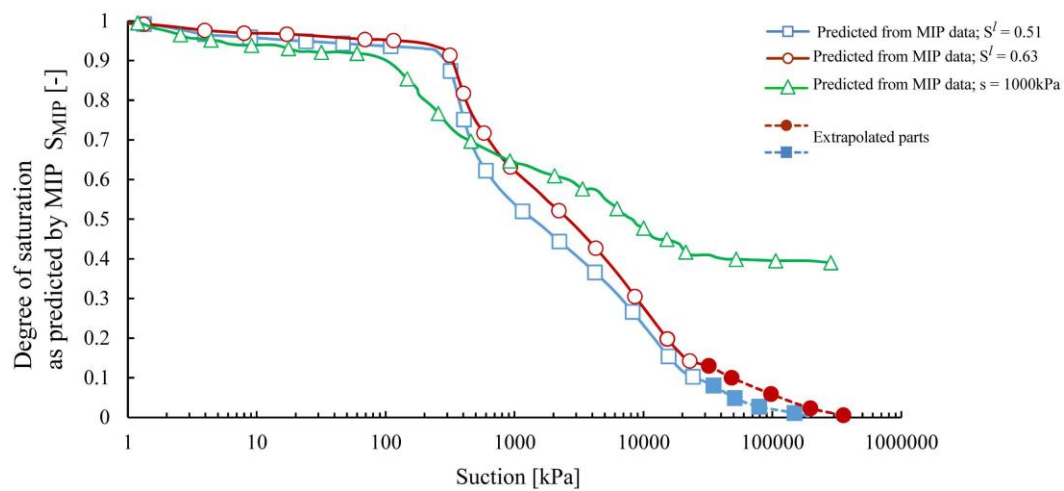




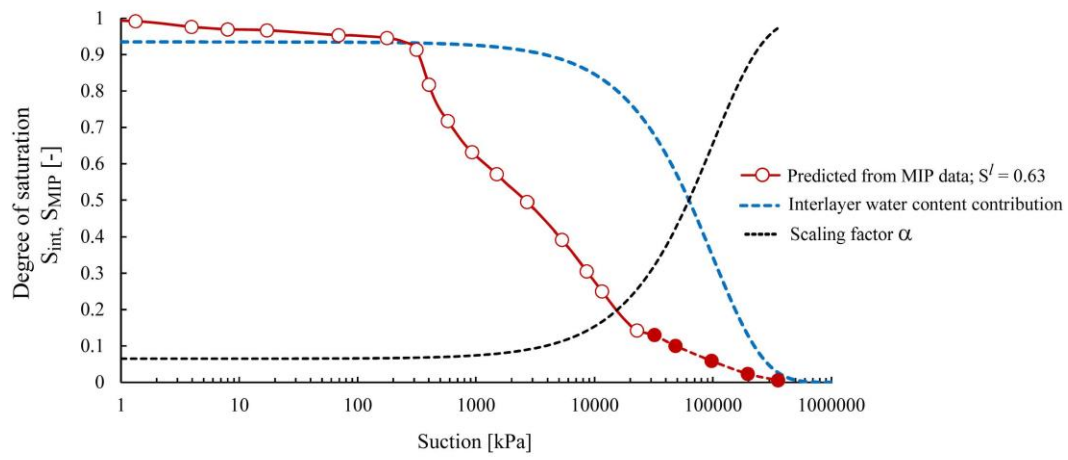
Abedfig20



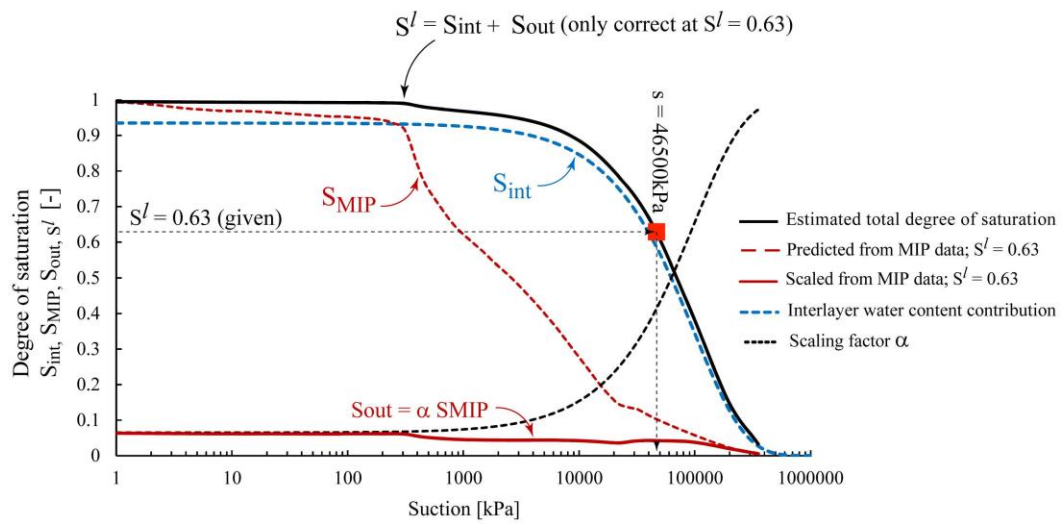
Abedfig21



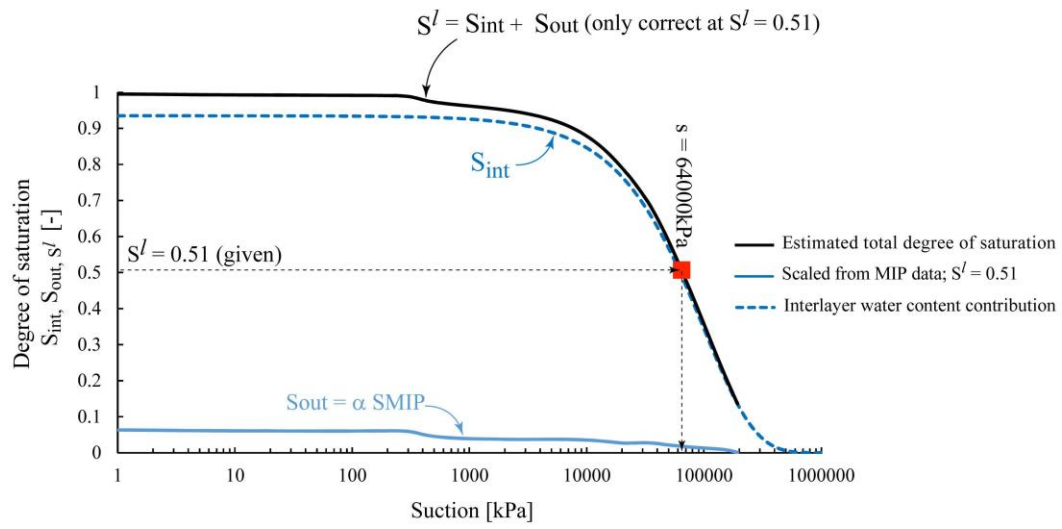
Abedfig22



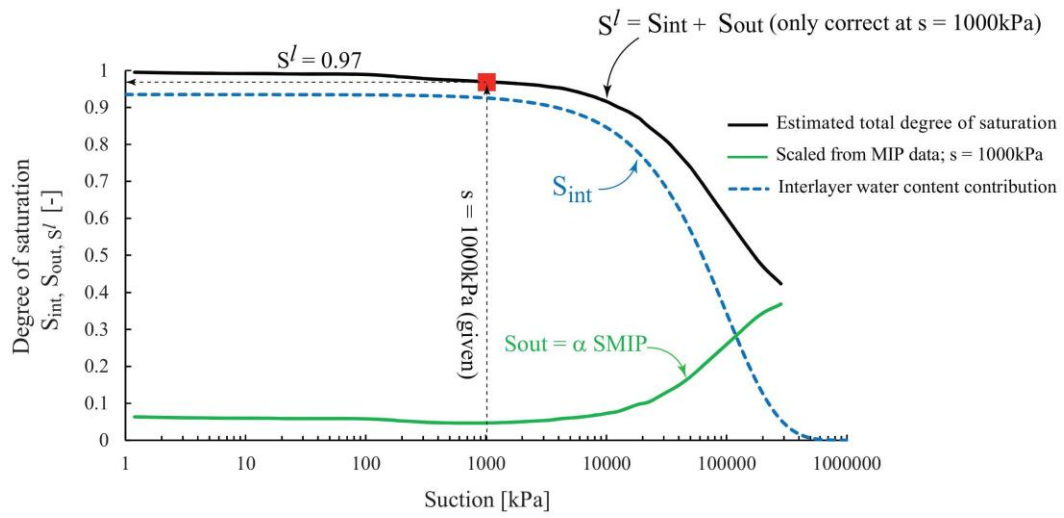
Abedfig23



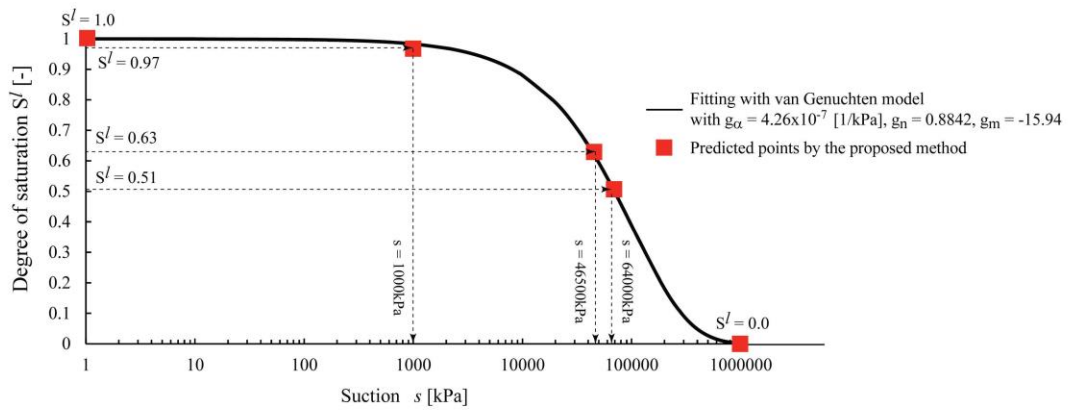
Abedfig24



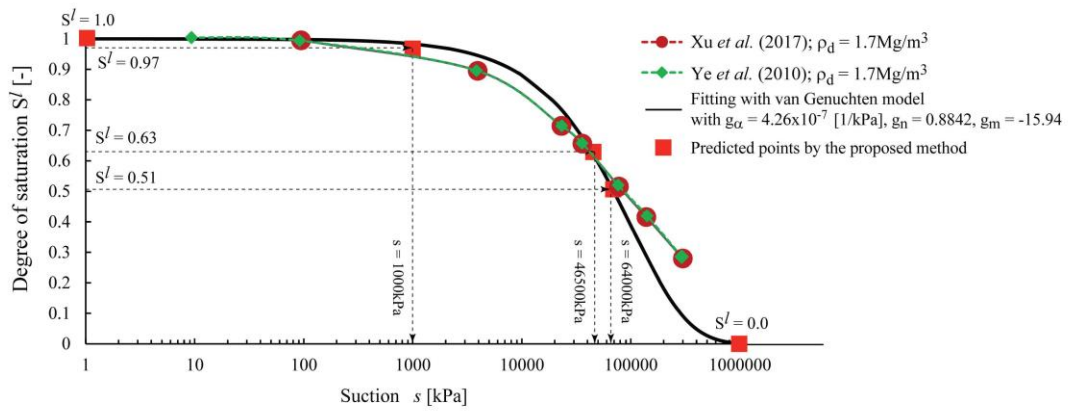
Abedfig25



Abedfig26



Abedfig27



Abedfig28